

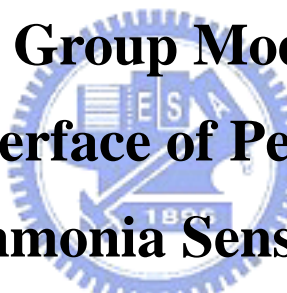
國立交通大學

光電工程研究所

碩 士 論 文

官能基修飾有機薄膜電晶體氣體感測  
之研究

**Functional Group Modification on  
Dielectric Interface of Pentacene-Based  
OTFTs for Ammonia Sensing Application**



研 究 生：吳權陵

指 導 教 授：冉曉雯 博士

中 華 民 國 九 十 七 年 八 月

# 官能基修飾有機薄膜電晶體氣體感測之研究

研究生:吳權陵

指導教授:冉曉雯 博士

國立交通大學

光電工程研究所碩士班

## 摘要

在此論文中,我們藉由修改官能基來得到有機薄膜電晶體(OTFTs) 氣體變化感覺能力。利用自組裝單層膜(SAM)的方式,在氧化層上分別修飾了三氨基丙基三乙氧基硅烷以及十八烷基三甲氧基硅烷。由於三氨基丙基三乙氧基硅烷以及十八烷基三甲氧基硅烷都是疏水層,因此會造成低表面能以利於五環素成長。因此氧化層與pentacene間的表面性質已經改變。而藉著改變表面態後的OTFTs來當作氣體感測器。對於氣體感應器,在我們的之前的研究,四點探針的方法用來研究寄生電阻以及薄膜電阻的改變。同時也顯示出,經過表面處理修飾後,pentacene薄膜電阻變化似乎已經變成主要因素,對於氣體感應而言。但是,寄生電阻是影響氣體感應的控制因素。相反結果,也可能由不同的SAMs解釋導致pentacene 結構或薄膜載子密度,進而影響OTFTs 與氣體間的反應。另外,多個參數,譬如載子遷移率、臨界電壓,和次臨界擺幅並且使用分析氣體感應互作用。基於在這個結果下,我們證明怎麼增加對專一氣體的感應能力,在藉由官能基修飾氧化層的方法下。在羅淵仁學長以及周政偉學長的指導下,一起合作進行此研究。

# **Functional Group Modification on Dielectric Interface of**

## **Pentacene-Based OTFTs for Ammonia Sensor**

### **Application**

**Student: Chuan-ling Wu**

**Advisor: Dr. Hsiao-Wen Zan**

Institute of Electro-Optical Engineering

National Chiao Tung University

### **Abstract**

IN this thesis, we modify the functional groups to obtain diversity of organic thin-film transistors (OTFTs) gas sensing ability. By using self-assembled monolayer (SAMs) treatment, the silicon oxide surface ( $\text{SiO}_2$ ) was modified by 3-amino-propyltriethoxysilane (APTES) and n-octadecyltrimethoxysilane (ODMS). Both ODMS and APTES (with amine groups) were hydrophobic, which served a low surface-energy surface for pentacene film growth. Therefore, the interface properties between pentacene film and  $\text{SiO}_2$  will be significantly changed. The OTFTs with interface modifications was then used as gas sensors. During gas sensing, in our previous reports, the gated-four-probes method was also used to analyze the changes of contact resistance and pentacene-film resistance. It was shown that with interface modifications, pentacene film resistance variation will become a key factor in gas sensing. However, the contact resistance was dominated factor that influenced gas

sensing. The contrary results can be explained by the different SAMs will result in different pentacene structure or thin-film carrier density, which influenced the OTFTs interaction to gases. Additionally, multiple parameters such as mobility, threshold voltage, and sub threshold swing were also used to analyze gas sensing interactions. Base on this result, we prove how to increase sensing ability of a specific material with functional groups modification on silicon oxide interface. In Cwei-Chou and Yuanren Lo's instruction, we cooperate together and finish this research.



## 誌謝

兩年的時間過的很快，回首兩年前，滿懷著夢想與期望來到交大。在交大的求學過程中，遇到了許多的考驗，這些考驗使自己在思想或能力上都成長許多。首先要感謝我的指導教授冉曉雯老師，感謝冉老師帶領我進入 OTFT 的世界，以及在研究路上不厭其煩的指導我。

感謝實驗室的博班學長：國錫學長、政偉學長、士欽學長，以及 楊裕雄實驗室的羅淵仁學長,在這兩年來的幫助與鼓勵。尤其是政偉學長以及淵仁學長，在我這兩年來的研究生涯裡，用心的教導我實驗方法並且辛苦地協助我完成我的碩士論文。感謝實驗室的同學：俊傑、志宇、旻君、武衛、和璉，這兩年來的互相打氣，互相砥礪。感謝實驗室的學弟妹們：淑玲、玉玫、鈞銘、慶能、達欣、威豪、建民、芳弘、煥之...等，在苦悶的研究生生活裡，添加了許多歡樂。

最後感謝我的父母、弟弟以及女友，感謝你們一路的陪伴與支持，沒有你們，就不會有今日的我。

# Contents

|                           |             |
|---------------------------|-------------|
| <b>Abstract (Chinese)</b> | <b>I</b>    |
| <b>Abstract (English)</b> | <b>II</b>   |
| <b>Acknowledgement</b>    | <b>IV</b>   |
| <b>Contents</b>           | <b>V</b>    |
| <b>Table Captions</b>     | <b>VII</b>  |
| <b>Figure Captions</b>    | <b>VIII</b> |

## **Chapter 1. Introduction**

|  |           |
|--|-----------|
| 1-1 Introduction of Organic Thin Film Transistors (OTFTs)        | <b>1</b>  |
| 1-2 Organic semiconducting materials and the transport mechanism | <b>2</b>  |
| 1-3 Surface treatment  | <b>8</b>  |
| 1-4 OTFT for gas sensing   | <b>9</b>  |
| 1-5 Motivation   | <b>10</b> |
| 1-6 Thesis Organization  | <b>10</b> |



## **Chapter 2. OTFT for gas sensing**

|   |           |
|---|-----------|
| 2-1 Brief review                            | <b>14</b> |
| 2-2 Sensing mechanisms                      | <b>15</b> |
| 2-2-1 Morphology effect                     |           |
| 2-2-2 Contact effect on nano-length devices |           |
| 2-2-3 Sensing Selectivity                   |           |
| 2-3 Immobilization of Bio-molecules         | <b>17</b> |

## **Chapter 3. Experiments Methods**

|  |           |
|--|-----------|
| 3-1 Device structures and fabrication                    | <b>22</b> |
| 3-1-1 Gated four-probes OTFTs for resistance measurement |           |
| 3-1-2 Preparation of Substrates                          |           |
| 3-1-3 Surface treatment                                  |           |
| 3-1-4 Growth of Thin Film and Electrodes                 |           |
| 3-2 Measurement Methods and Parameters extraction        | <b>25</b> |
| 3-2-1 Mobility   |           |

|                            |           |
|----------------------------|-----------|
| 3-2-2 Threshold voltage    |           |
| 3-2-3 On/Off current ratio |           |
| 3-2-4 Subthreshold swing   |           |
| 3-2 Gas-Sensing system     | <b>27</b> |

## **Chapter 4. Result and Discussion**

|   |           |
|---|-----------|
| 4-1 SAM with APTES/ODMS   | <b>32</b> |
| 4-1-1 Percentage control  |           |
| 4-1-2 Molecule Immobilization   |           |
| 4-2 Material and electrical analysis on SAM-OTFTs                       | <b>33</b> |
| 4-2-1 AFM analysis of SAM quality                                       |           |
| 4-2-2 Electrical Characteristics of OTFTs with distinct SAM-dielectrics |           |
| 4-3 Effects of ammonia (NH <sub>3</sub> ) on Gated four-probe SAM-OTFTs | <b>35</b> |
| 4-3-1 Id-Vg curve variation   |           |
| 4-3-2 Contact resistance variation                                      |           |
| 4-3-3 Threshold voltage and mobility variation                          |           |

## **Chapter 5. Conclusion and Future work**

|                                |           |
|--------------------------------|-----------|
| 5-1 Conclusion and future work | <b>54</b> |
|--------------------------------|-----------|

|                   |           |
|-------------------|-----------|
| <b>References</b> | <b>56</b> |
|-------------------|-----------|

|                |           |
|----------------|-----------|
| <b>Profile</b> | <b>63</b> |
|----------------|-----------|

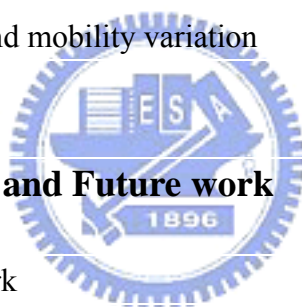


## Table Captions

Table I Summary of reviewed OFET sensors

Table II The surface roughness of ODMS, ODMS mixed with APTES,  
APTES-dipped SiO<sub>2</sub>

Table III The comparison of ODMS and APTES -OTFTs electrical properties





# Figure Captions

## Chapter 1

**Fig. 1.1** The applications of plastic transistors: flexible displays, smart cards, RFID tags.

**Fig. 1.2** Semilogarithmic plot of mobility vs. year.

**Fig. 1.3** Molecular structure of (a) sexithiophene and (b) pentacene.

**Fig. 1.4** Energy band diagram of pentacene

**Fig. 1.5** Chemical structure of APTES and ODMS - SAMs

## Chapter 2

**Figure 2.1.** Sensing data of  $I_{ds}$  (normalized to that measured just before the analyte was delivered) for 80 nm pentacene grain size and different nanoscale channel lengths (same W/L of 10), measured at  $V_g = V_{ds} = V_{side} = -2.5$  V (two side guards were kept at the same potential as the drain),  $d$  distance from syringe nozzle to device = 2 mm,  $v$  analytic flux = 45 ml/min

**Figure 2.2** Map illustrating the effect of 16 analytes on 11 sensor materials. Black indicates that data are not available and white indicates negligible response. Positive changes in sensor current are shown in shades of blue while decreases are shown in shades of red.

## Chapter 3

**Figure 3.1.** (a) Top view of a field-effect device. (b) Schematic voltage drop along the channel for an OTFT biased in the linear region of device operation. The potential drop between the voltage-probing electrodes is assumed to be linear for the evaluation of the mobility from the four-terminal measurement.

**Fig. 3.2** The device structure of SAM-treated OTFTs.

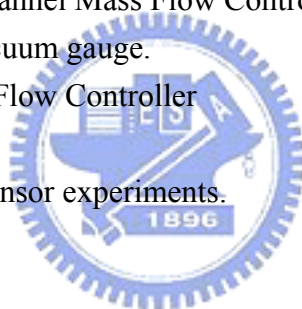
**Fig. 3.3** sensor measurement system.

**Fig. 3.4** analyte controll system.

(a) There is a four channel Mass Flow Controller (MFC) Readout Power Supply, and a vacuum gauge.

(b) There is a Mass Flow Controller

**Fig. 3.5** Chamber used for sensor experiments.



## Chapter 4

**Fig.4.1** The contact angle of the de-ionized water on ODMS-treated SiO<sub>2</sub> surface, and on APTES-treated SiO<sub>2</sub> surface, respectively.

**Fig.4.2 (a)** The amine groups of APTES can covalent bonding with anti-body.

(b) The amine groups of APTES can covalent bonding with bovine serum albumin (BSA)

(c) Atomic force microscope (AFM) images of SAM-dipped SiO<sub>2</sub> dielectric for ODMS and APTES

(d) pentacene AFM image on SAM-dipped SiO<sub>2</sub> layer for ODMS and APTES

**Fig.4.3** Transfer characteristics of OTFT with treated ODMS/APTES dielectric

**Fig.4.4 (a)** Electrical characteristics of ODMS-OTFTs in 0.5ppm NH<sub>3</sub> in 5mins, 10mins, and 20mins.

**(b)** Electrical characteristics of APTES-OTFTs in 0.5ppm NH<sub>3</sub> in 5mins, 10mins, and 20mins

**Fig.4.5(a)** field-effect mobility and threshold voltage of ODMS-OTFTs in 0.5ppm NH<sub>3</sub> in 5 mins, 10mins, and 20mins.

**(b)** field-effect mobility and threshold voltage of APTES-OTFTs in 0.5ppm NH<sub>3</sub> in 5 mins, 10mins, and 20mins.

**Fig.4.6 (a)** Electrical characteristics of ODMS-OTFTs in NH<sub>3</sub>.

**(b)** Electrical characteristics of APTES-OTFTs in NH<sub>3</sub>.

**(c)** the change of maximum on drain-current ( $I_D$ ) of ODMS and APTES-OTFT versus NH<sub>3</sub> concentration

**Fig.4.7** The  $R_{cont}$  and  $R_{film}$  are plotted as a function of gate-voltage minus threshold-voltage ( $V_G - V_{th}$ ), respectively.

**Fig. 4.8 (a)** For ODMS-OTFTs, the percentage (%) of  $R_{cont}$  and  $R_{film}$  versus injected NH<sub>3</sub>.

**(b)** For APTES-OTFTs, the percentage (%) of  $R_{cont}$  and  $R_{film}$  versus injected NH<sub>3</sub>.

**Fig. 4.9** The threshold voltage shift ( $\Delta V_{th}$ ) of ODMS and APTES-OTFTs is plotted as a function of NH<sub>3</sub> concentration.

**Fig. 4.10** The field-effect mobility of ODMS and APTES-OTFTs is plotted as a function of NH<sub>3</sub> concentration.

**Fig. 4.11** The subthreshold swing ( $S.S.$ ) of ODMS and APTES-OTFTs is plotted as a function of NH<sub>3</sub> concentration.

**Fig. 4.12** The sensing mechanism during NH<sub>3</sub> in the chamber

# Chapter 1

## Introduction

### 1.1 Introduction of Organic Thin Film Transistors (OTFTs)

“Plastic transistors” open the future of flexible displays, smart cards, radio frequency (RF) identification tags, as well as light-emitting diodes (LED) and lasers [1]. Rapid progress in this field has been achieved by improving the material properties and the process techniques.

As for the application of electronics, the organic active layer has attained a mobility of  $1\text{cm}^2/\text{Vs}$  and a switching speed of  $10^8$  Hz, which is comparable to amorphous hydrogenated silicon (a-Si:H)[2]. Since the late 1940s, there has been a lot of research on the development of organic semiconductor [3]. These organic semiconductors are small molecules and polymers, which have alternative single or double-bond in common. This is because of the large  $\pi$ -conjugation length along the long axis of the molecules and closed  $\pi$ -stacking are the key factors of high carrier mobility [3].

Similar to inorganic semiconductors, organic ones can function as p-type or n-type. However, most reported high-mobility organic semiconductors are p-type material. Among the p-type material, pentacene ( $\text{C}_{14}\text{H}_{22}$ ), a rod-like aromatic molecule composed of five benzene rings, shows the highest mobility ( $>1\text{cm}^2/\text{v-sec}$ ),

owing to highly ordered films with proper dielectric properties and growth conditions[4].

## 1.2 Organic semiconducting materials and the transport mechanism

Organic materials such as polythiophene,  $\alpha$ -sexithiophene ( $\alpha$ -6T) have been investigated for use in field effect transistors (FETs) [5]. Polycrystalline molecular solids such as  $\alpha$ -sexithiophene ( $\alpha$ -6T) or amorphous/semi-crystalline polymers such as polythiophene or acenes such as pentacene, teracene show the highest mobility [6].

Figure 1.2 shows the evolution of organic materials and the improvement in their

mobility over the years [7]. Pentacene based FETs show the high mobility and have been extensively studied. Pentacene is made up of five benzene rings as shown in Fig.

1.3 .Pentacene has a sublimation temperature of 300°C . Well ordered pentacene films can be deposited at low temperatures making it suitable for deposition on plastic substrates.

Organic conjugated materials used in OTFTs can be generally divided into two groups. Among the semiconductors, one group is the polymers and the other is the oligomers. The polymers are formed by a repeating chain of hydrogen and carbon in various configurations with other elements, but they have relatively poor mobilities ( $4 \times 10^{-2} \text{ cm}^2/\text{Vs}$  [8]). The oligomers are held together by weak Van der Waal forces and thermal-evaporated with good ordering. Devices fabricated with oligomers have

higher mobilities (1.5 cm<sup>2</sup>/Vs [9]). The organic materials can function either as p-type or n-type. In p-type semiconductors, the majority carriers are holes; while in n-type the majority carriers are electrons. Among, p-type semiconductors are the most widely studied organic semiconductors. Recently, many molecular semiconductors, such as pentacene, thiophene oligomers, and regioregular poly(3-alkyl-thiophene) are proposed. The pentacene (C<sub>22</sub>H<sub>14</sub>) is a promising candidate for future electronic devices and an interesting model system, due to its superior field effect mobility and environmental stability [10].

Pentacene is one of the popular materials in OTFTs. Its mobility has reached the fundamental limit (>3cm<sup>2</sup>/Vs) [11, 12] which is obtained with a single crystalline at room temperature. The mobility of pentacene is comparable to that of amorphous silicon which is widely developed and used in active matrix liquid crystal displays (AMLCD) and the other electronic applications.

Pentacene is an aromatic compound with five condensed benzene rings and therefore, the chemical formula is C<sub>22</sub>H<sub>14</sub> with molecular weight 278.3. The volume of the unit cell is about 705Å [11]. The permittivity is 4 [12], and the electron affinity is about 2.49eV. Silinish *et al.* determined the adiabatic energy gap ( $E_G^{Ad}$ ) by using the threshold function of intrinsic photoconductivity in pentacene[13]. The second transition is from the excited state to the ionic state, which is called the optical energy

gap ( $E_G^{opt}$ ). According to Fig. 1.4, the adiabatic energy gap as 2.47eV and the optical energy gap as 2.83eV are recorded [14]. Pentacene is used as an active layer. Its purity leads to longer diffusion length for the charge transporting with less interaction with the lattice. Furthermore, the impurities in the material tend to chemically combine with the organic semiconductor material which leads to irregularities in the band gap [15]. Therefore, the thermal evaporation is carried out under high or ultra high vacuum conditions to avoid the impurities and increase the quality of the material. It is well known that the deposition temperature, deposition pressure, and deposition rate are the three critical parameters to the organic film quality. Lower deposition rate and appropriate deposition temperature is expected to result in better ordering of the organic molecules, thin-film phase formation of pentacene film, and the better performance [16]. In OTFTs, the roughness has a influence on the morphology, whereas the films on the smooth thermal oxide are in generally highly ordered. The surface chemistry also is a typical issue to organic devices. Changing surface wettability as a hydrophobic surface by surface treatment leads to mobilities increasing [17].

Carrier transportation in the organic semiconductors have been investigated on the theory and modeling in the past years [18]. Recently, two principal types of theoretical model are used to describe the transport in organic semiconductors: “The

band-transport model” and “The hopping models”. However, band transport may not suit for some disordered organic semiconductors, in which carrier transport is govern by the hopping between localized states. Hopping is assisted by phonons and the mobility increases with temperature. Typically, the mobility is very low, usually much lower than  $1\text{cm}^2/\text{V}\cdot\text{sec}$ . The boundary between “band transport” and “hopping” is divided by materials mobilities ( $\sim 1\text{cm}^2/\text{V}\cdot\text{sec}$ ) at room-temperature (RT) [19]. Many kinds of polycrystalline organic semiconductors, such as several members of the acene series including pentacene, rubrene, have RT mobility over the boundary [20]. Sometimes, temperature-independent mobility was found in some polycrystalline pentacene devices [21]. Thus, this observation argued that the simply thermal activated hopping process governed the whole carrier transport behaviors in high quality polycrystalline pentacene film; despite that the temperature independent mobility has been observed in exceptional cases [21].

Finally, the exact nature of the charge carrier transport in organic molecular crystals is still not well-understood, which has been the focus in many theoretical studies [22].

In the past 20 years, a great deal of progress has been made in improving the field-effect mobilities of OFETs [23]. It has also been demonstrated that the properties of charge transport in conjugated molecules are intrinsically correlated with their



crystalline structure, where the  $\pi$  delocalized carriers are responsible for the intra-molecular conduction. However, the nature of van der Waals bonding between discrete molecules is thought to be the limitation of the carrier transport, and the transport is usually described by “localized model. Thus, the charged carrier transport must be described by different models than those in covalently bonded semiconductors.

Recently, two principal types of theoretical model are used to describe the transport in organic semiconductors: “The band-transport model” and “The hopping models”. However, band transport may not suit for some disordered organic semiconductors, in which carrier transport is govern by the hopping between localized states. Hopping is assisted by phonons and the mobility increases with temperature. Typically, the mobility is very low, usually much lower than  $1\text{cm}^2/\text{V}\cdot\text{sec}$ . The boundary between “band transport” and “hopping” is divided by materials mobilities ( $\sim 1\text{cm}^2/\text{V}\cdot\text{sec}$ ) at room-temperature (RT) [24]. Many kinds of polycrystalline organic semiconductors, such as several members of the acene series including pentacene, rubrene, have RT mobility over the boundary [25]. Sometimes, temperature-independent mobility was found in some polycrystalline pentacene devices [26]. Thus, this observation argued that the simply thermal activated hopping process governed the whole carrier transport behaviors in high quality

polycrystalline pentacene film; despite that the temperature independent mobility has been observed in exceptional cases [27].

The understanding of carrier transport in single-crystal of organic semiconductors will help us to describe the transport mechanism in polycrystalline organic semiconductors. The coherent band-like transport of delocalized carriers becomes the prevalent transport-mechanism in the single crystals of organic semiconductors, such as pentacene, tetracene, under the low-temperature environments. A very high hole mobility values has been measured by time-of-flight experiments. Thus, the temperature dependence of the carrier mobility was found below 100K and following with a power law of  $\mu \propto T^{-n}$ ,  $n \sim 1$ , in single crystals of organic semiconductors, consistent with the band-transport model. However, between 100K and 300K, the carrier mobility show a constant value, that has been described as the superposition of two independent carrier transport mechanisms. The first mechanism was small molecular polaron (MP). According to this model, the carriers were treated as the heavy; polaron-type; quasi-particles. It is formed by the interaction of the carriers with intra-molecular vibrations of the local lattice environment, and move coherently via tunneling. In this model, the mobility follows the power law  $\mu_{MP} = aT^{-n}$ . The other involves a small lattice polaron (LP), which moves by thermally activated hopping and exhibits a typical exponential

dependence of mobility on temperature:  $\mu_{LP} = b \exp[-E_a/kT]$ . The superposition of these two mechanisms could get a good consistence with experimentally measurement of temperature-dependence mobility from room temperature to Kelvin degrees (K).

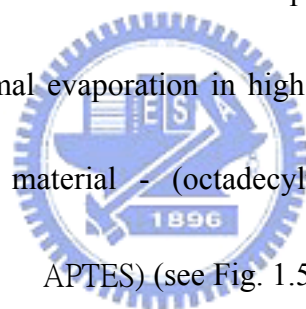
Finally, the exact nature of the charge carrier transport in organic molecular crystals is still not well-understood, which has been the focus in many theoretical studies.

### 1.3 Surface treatment

Several researchers had verified the hydrophobic surface was more suitable for organic film deposition [28]. Since the hydrophobic polymer dielectric has lower or similar surface energy to organic films. The similar concept was also realized by self-assembled monolayer (SAM) on inorganic dielectrics. If the inorganic dielectrics with lower surface-energy, that may provide better performance and resulted in lower interface traps in OTFTs [29]. The surface properties such as frictional or abrasion, permeability, insulating properties, wettability and chemical reactivity are strongly dependent on a molecular aggregation state of the surface [30, 31]. Therefore, the control of a molecular aggregation state on the film is important to construct a highly functionalized surface. One of the most effective ways of studying surface properties is contact angle measurement. The contact angle is the angle

between the tangent to the drop's profile and the tangent to the surface at the intersection of the vapor, the liquid, and the solid. The contact angle is an index of the wettability of the solid surface. A low contact angle between solid surface water-drop indicates that the surface is hydrophilic and has a high surface energy. On the contrary, a high contact angle means that the surface is hydrophobic and has a low surface energy. The surface free energy was traditionally quantified by contact angle measurements [32, 33].

In this study, we fabricated the electrical properties of the OTFTs using pentacene fabricated by thermal evaporation in high vacuum with the two kinds of dielectric surface treatment material - (octadecyltrimethoxysilane, ODMS) and (3-Aminopropyltriethoxysilane, APTES) (see Fig. 1.5).



#### **1.4 OTFTs for gas-sensing**

For the next generation of sensor applications on medical diagnostics, food monitoring, and chemical or biological warfare etc.; portable, low cost, and low power-consumption will be important demands. As for these demands, the OTFT should be an important candidate due to its flexibility and its simple fabrication process. Therefore, the studies of organic thin-film transistors (OTFTs) to physical, chemical [34], and biological sensors [35] will become an important object.

Recently, OTFTs are proposed to act as gas sensors. When OTFTs exposed to

gaseous species, five parameters: the turn-on current ( $I_{on}$ ), the turn-off current ( $I_{off}$ ), the threshold-voltage ( $V_{th}$ ), the field-effect mobility ( $\mu_{eff}$ ) and the subthreshold-swing ( $S.S.$ ), are used to estimate the gaseous interaction in OTFTs. By this way, a “multi-dimensional” gas sensor can be realized as a single OTFT.

## 1-5 Motivation

How to promote the sensing qualitative ability of OTFTs sensor is always an important topic. We propose modifying dielectric surface by different functional groups of SAM can change characteristics of gas sensing.

SAM was more hydrophobic and the surface free energy was similar to that of the pentacene film. Besides, we change the functional groups of SAM to change ammonia sensor ability. If we can obtain different gas sensing characteristics modified by different functional groups, we can attain the sensing qualitative ability.

## 1-6 Thesis Organization

In Chapter 1, we describe the introduction of OTFTs, Surface treatment and motivation of the thesis. In Chapter 2, we introduce sensing mechanisms, and immobilization of Bio-molecules. In Chapter 3, the fabrication and the structure of OTFTs, and parameter extraction are presented. In Chapter 4, Self-Assembly Monolayer (SAM) and surface energy, electrical properties of SAM-treated OTFTs, and effects of ammonia ( $NH_3$ ) on Gated four-probe OTFTs are investigated. Finally, we describe the conclusion and future work in Chapter 5.



**Figure 1.1** The applications of plastic transistors: flexible displays, smart cards, RFID tags.

[Adapted from <http://tech.sina.com.cn/digi/2006-04-20/1204911539.shtml>]

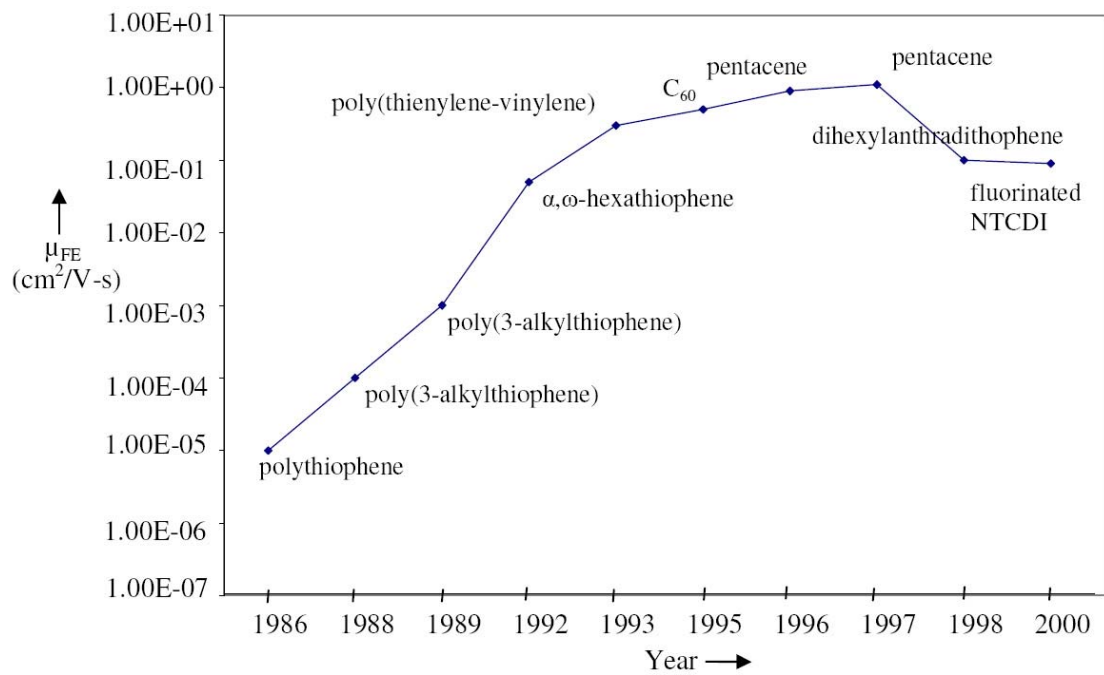


**Fig. 1.2** Semilogarithmic plot of mobility vs. year.

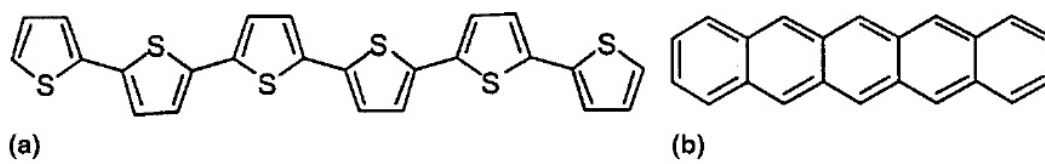


**Fig. 1.3** Molecular structure of (a) sexithiophene and (b) pentacene.

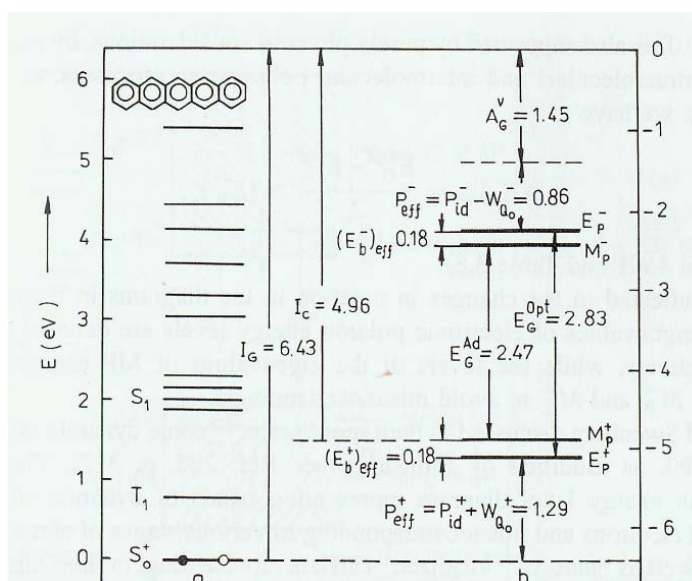


**Fig. 1.4** Energy band diagram of pentacene

3-Aminopropyltriethoxysilane (APTES)    octadecyltrimethoxysilane (ODMS)

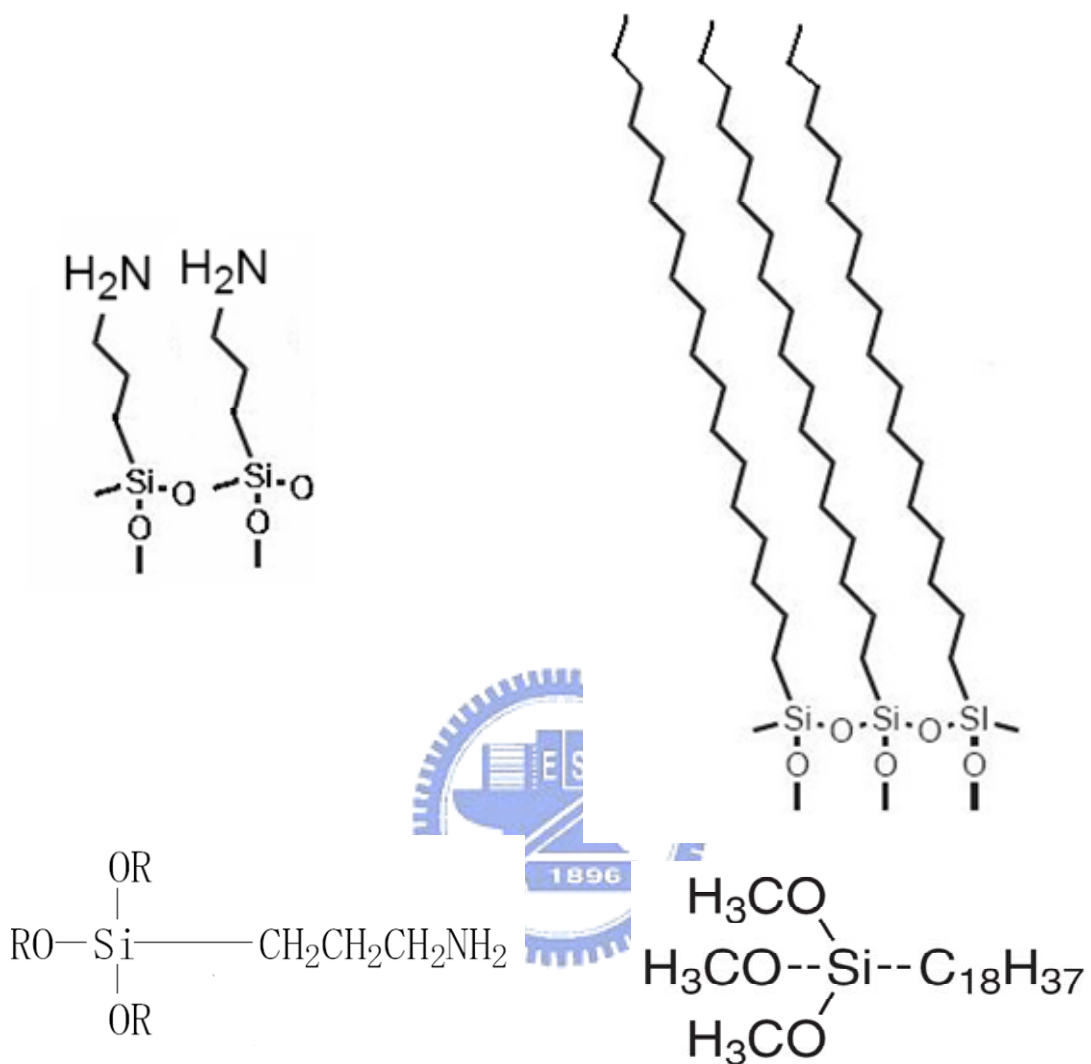


**Fig. 1.5** Chemical structure of APTES and ODMS - SAMs



# Chapter 2

## OTFTs for gas sensing

### 2-1 Brief Review

Organic thin-film transistors (OTFTs) offer a great deal of promise for applications in chemical and biological sensing. For a broad range of sensing applications (e.g., medical diagnostics, food monitoring, detection of chemical, biological warfare agents, etc.), there is a demand for small, portable, and inexpensive sensors. OTFTs have many advantages over other types of sensors that may allow them to meet this need. Organic semiconductors can be deposited using low-temperature processes on a variety of substrates, including mechanically flexible ones. As a result, low-cost fabrication techniques can be used to produce OTFTs. Miniaturization of these devices is straightforward, so portability, small sample volumes, and arrays with many elements are achievable. In addition, they provide a response (current change) that is easy to measure with simple instrumentation. With these advantages, it is feasible that single-use, disposable sensors could be realized using OTFTs.

OTFTs can be roughly classified into two primary categories: organic field-effect transistors (OFETs) and organic electrochemical transistors (OECTs) (including ISOFETs) OECTs exhibit much lower operating voltages than OFETs, but due to the

movement of ions involved in OECTs, their switching times are considerably slower (on the scale of seconds or longer) than those for OFETs (on the scale of milliseconds or shorter). In this paper, [34] they show the chemical and biological sensors based on OTFTs. (see Table I)

## **2-2 Sensing Mechanisms**

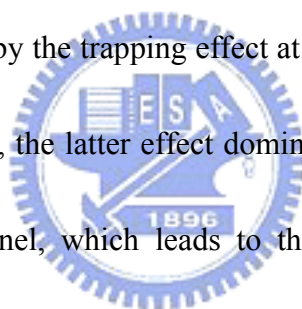
### **2-2-1 Morphology effect**

Grain boundaries (GBs) play a critical role in OFET sensing. The grain size of the corresponding film was varied by changing the substrate temperature during deposition. According to the images from transmission electron microscope (TEM) from different substrate temperatures, Torsi et al. indicate that the response is strong for the low-temperature film one, which has more grain boundaries. However, the response is weak for the high-temperature one, which has fewer grain boundaries and a more compact structure. That implies for alcohols, the response of the sensor depends on interaction at grain boundaries. [36]

### **2-2-2 Contact effect on nano-length devices**

The modeling for the mechanism of the sensing response will be published elsewhere. [37] Here, the reference briefly proposes the concept of the sensing mechanism of polycrystalline organic thin-film dependent on the channel length relative to grain sizes. In the organic semiconductor layer, both grains and grain

boundaries could be affected by the analyte molecules. Due to their dipole nature, the analyte molecules airborne on grain boundaries will trap the mobile charge carriers from the channel. [38] [39] Meanwhile the analyte (1-pentanol) interacting with the semiconductor (pentacene) grains will result in excess holes through chemical processes that are not completely understood. We propose that the overall sensing response is the result of a combination of these two competing effects. For a longer channel relative to grain sizes, there are enough grain boundaries inside the channel so that the former effect is dominant and the overall sensing response is the current decreasing (mobility reduced by the trapping effect at grain boundaries). For a shorter channel relative to grain sizes, the latter effect dominates due to very few number of grain boundaries inside channel, which leads to the current increasing by excess charges from the interaction between grains and the analyte. The result is shown in Fig.



2.1

### **2-2-3 Sensing Selectivity**

To realize selective gas detection, sensor arrays are often constructed, i.e. several sensors showing different patterns of gas sensitivity are selected and simultaneously operated. Signal evaluation algorithms ranging from partial least squares methods to neural networks with fuzzy preprocessing are used to identify the

type of gases presented and to calculate their concentrations. A simple technique to obtain an array using one sensor is to modulate the operating temperature to different define levels.

In the research of Crone et al. [40], they adopt eleven different organic thin films to make OTFT and observe the reaction of these OTFTs to sixteen different gases. The result is shown in Fig. 2.2 and it also reveals that OTFTs apply to electronic nose. Then, in 2005 year Liao et al. submitted that concept of application of OTFTs on electronic nose. [41] They proposed three different active materials including P3HT, pentacene, and P3OT to make OTFTs and show the sensing gas selectively for these OTFTs.



### **2-3 Immobilizations of Bio-molecules**

Self-assembled monolayer (SAM) technology provides a powerful tool for generating monolayers of biological molecules on various substrates. The formation of such monolayers offers great versatility in terms of the sophisticated bio-recognition, which might provide a method for the in vitro development of biosurfaces that are able to mimic naturally occurring molecular recognition process [42]. SAMs also permit reliable control over the packing density and the environment of an immobilized recognition center or multiple centers on a substrate surface [43].

In the paper, they demonstrate a novel DNA hybridization detection method with organic thin film transistors.[44] DNA molecules are immobilized directly on the surface of organic semiconductors, producing an unambiguous doping-induced threshold voltage shift upon hybridization. With these shifts, single-stranded DNA (ssDNA) and double-stranded DNA (dsDNA) are differentiated successfully.

In our research, we try to immobilize BSA on the SAM treated surface, and observe that BSA bond with APTES .Then, we make OTFTs treated by SAM to sense gas and try to increase the sensing selectivity of OTFTs for ammonia. Finally, we expect to immobilize DNA on the SAM treated surface and detect Biological member.



**Table I** Summary of reviewed OFET sensors

| Active layer                            | Recognition element  | Analytes   |
|---|--|--|
| <b>OTFTs</b>                            |  |  |
| Phthalocyanines                         |  | <i>Oxygen, iodine, bromine, NO<sub>2</sub>, ozone, alcohols, ketones, thiols, nitriles, esters, ring compounds, lactic acid, pyruvic acid</i>  |
| Naphthalene tetracarboxylic derivatives |  | <i>Nitrogen, oxygen, water vapor, alcohols, ketones, thiols, nitriles, esters, ring compounds</i>  |
| Pentacene                               |  | <i>Water vapor, 1-pentanol, aqueous analytes</i>   |
| Oligothiophenes                         |  | <i>Alcohols, ketones, thiols, nitriles, esters, ring compounds, lactic acid, glucose</i>   |
| Polythiophenes                          | Alkyl or alkoxy side chains  | <i>Ammonia, water vapor, chloroform, alcohols, ketones, thiols, nitriles, esters, ring compounds, alkanes</i>  |
| Poly(phenylene ethynylene)              | Enantioselective pendant groups  | <i>Volatile chiral molecules</i>   |
| <b>ISOFETs</b>                          |  |  |
| Pentacene                               |  | H <sup>+</sup>   |
| Poly(3-hexylthiophene)                  | Proton-sensitive dielectric layer, glucose oxidase   | H <sup>+</sup> , glucose   |
| <b>OEFTs</b>                            |  |  |
| Poly pyrrole                            | Disphorase, penicillinase membrane   | NADH, penicilline, H <sup>+</sup>  |
| Poly(3-hexylthiophene)                  | Platinum particles   | H <sup>+</sup> , IrCl <sub>6</sub> <sup>2-</sup> , O <sub>2</sub> , H <sub>2</sub>   |
| Polyaniline                             | Moisture-sensitive solid-state electrolyte, crown ether, glucose oxidase, horseradish peroxidase, urease, lipase | H <sup>+</sup> , Ru(NH <sub>3</sub> ) <sub>6</sub> <sup>3+/2+</sup> , Fe(CN) <sub>6</sub> <sup>3-/4-</sup> , <i>water vapor</i> , SO <sub>2</sub> , K <sup>+</sup> , glucose, hydrogen peroxide, urea, triglycerides |
| Polyaniline composites                  | Glucose oxidase  | Glucose, NADH  |
| Modified polyaniline                    | Horseradish peroxidase   | Hydrogen peroxide  |
| Polycarbazole                           |  | Cu(II) ions  |
| PEDOT                                   | IgG antibodies, DNA  | IgG antibodies, DNA  |
| PEDOT/PSS                               | Glucose oxidase  | <i>Water vapor, glucose</i>  |

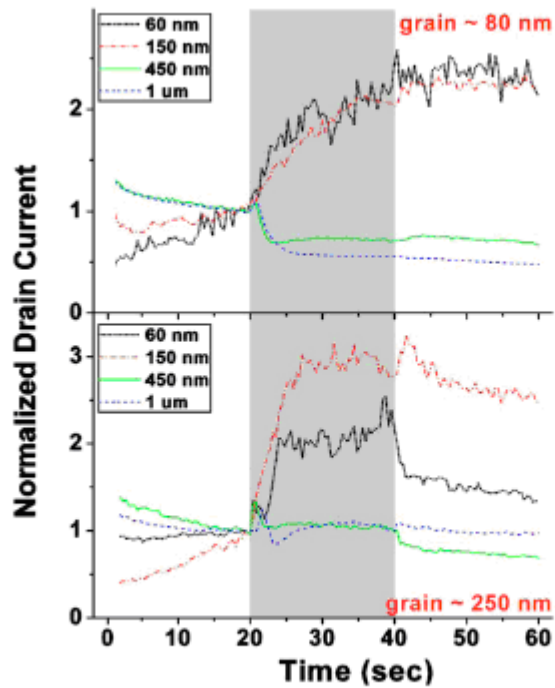


**Figure 2.1.** Sensing data of  $I_{ds}$  (normalized to that measured just before the analyte was delivered) for 80 nm pentacene grain size and different nanoscale channel lengths (same W/L of 10), measured at  $V_g = V_{ds} = V_{side} = -2.5$  V (two side guards were kept at the same potential as the drain),  $d$  distance from syringe nozzle to device = 2 mm,  $v$  analytic flux = 45 ml/min.

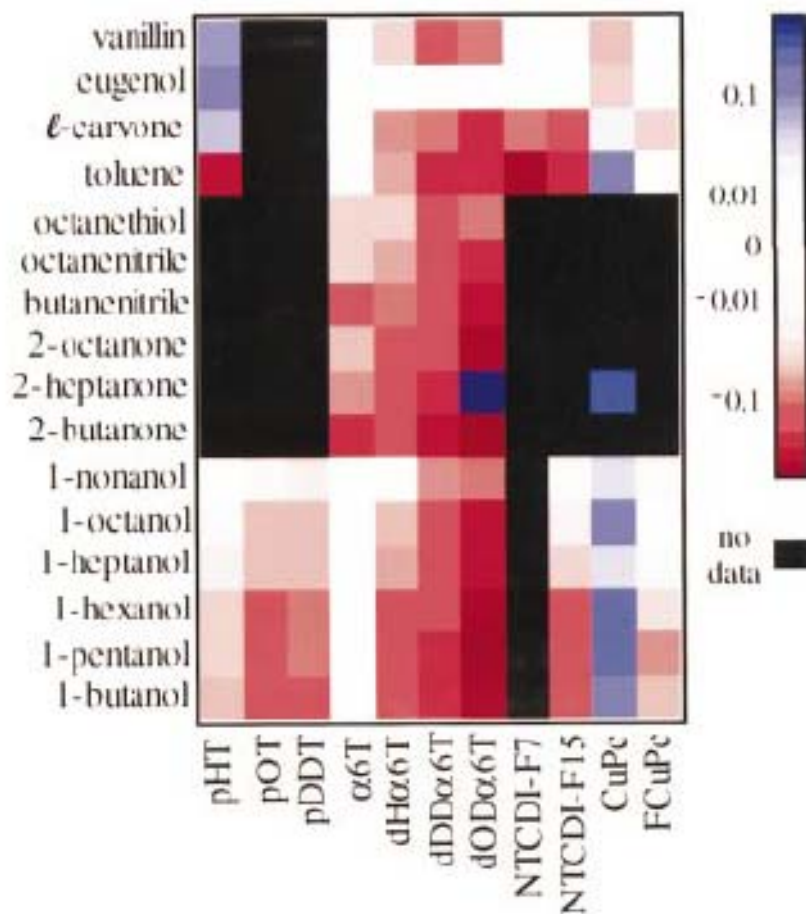


**Figure 2.2** Map illustrating the effect of 16 analytes on 11 sensor materials. Black indicates that data are not available and white indicates negligible response. Positive changes in sensor current are shown in shades of blue while decreases are shown in shades of red.



# Chapter 3

## EXPERIMENT METHODS

### 3-1 Device Structures and Fabrication

#### 3-1-1 Gated four-probes OTFTs for resistance measurement

Gated four-probe OTFTs electrical measurements were carried out using a Keithley 4200-SCS semiconductor parameter analyzer. In the four-terminal measurements (Fig.3.1 (a)) the voltage drops  $V_1$  and  $V_2$  between the source contact and the two voltage-probing electrodes were measured separately, with two Kelvin-probes SMUs set current less than  $10^{-14}$  Amps and measure the voltage. As shown in Fig. 3.1(b) (an idealized depiction of the change in potential through the device when biased in the linear region of device operation), the potential drop between the voltage probes is assumed to be linear for  $|V_{DS}| < |V_{GS} - V_T|$  (where  $V_T$  is the threshold voltage,  $V_{GS}$  is the gate-source voltage, and  $V_{DS}$  is the drain-source voltage), the field-effect mobility is given by

$$\mu = \frac{L}{W} \times \frac{1}{C_i} \times \frac{1}{V_{DS}} \times \frac{\partial I_D}{\partial V_{GS}} \quad (1)$$

where  $C_i$  is the gate insulator capacitance per unit area about  $3.45 \times 10^{-8}$  F/cm<sup>2</sup>.

Knowing the channel potential at two points,  $V_1$  and  $V_2$ , a linear extrapolation of the potential profile to each contact was performed. The potential drops at the source and drain,  $\Delta V_S$ ,  $\Delta V_D$  and  $\Delta V_{Film}$ , were calculated according to the following

equations:

$$\Delta V_s = \left[ V_2 - \frac{(V_1 - V_2)}{(L_2 - L_1)} (L - L_2) \right] - V_s \quad (2)$$

$$\Delta V_D = V_D - \left[ V_2 + \frac{(V_1 - V_2)}{(L_2 - L_1)} L_2 \right] \quad (3)$$

$$\Delta V_{Film} = \frac{(V_1 - V_2)}{(L_2 - L_1)} L \quad (4)$$

Where  $V_D, V_1$  and  $V_2$  are the voltages at the source, drain, and potential probes, respectively.  $L_1, L_2$  and  $L$  are the distances from the drain electrode to the first potential probe, the second potential probe, and the source electrode, respectively.

Where  $\Delta V_{Film}$  is the actual voltage drop across the film.

With the knowledge of the total current flowing through the device and the potential drops across the film and contacts, the resistance of the source contact, drain contact, and the film can be calculated using Ohm's Law, when devices operation in linear region.

$$R_s = \frac{\Delta V_s}{I_D} \quad (5)$$

$$R_D = \frac{\Delta V_D}{I_D} \quad (6)$$

$$R_F = \frac{\Delta V_F}{I_D} \quad (7)$$

### 3-1-2 Preparation of Substrates

In this study, the OTFT devices we used are top-contact structures. A p-type, single crystal silicon wafer (100) was used as the substrate and the gate electrode. After RCA cleaning, a 1000Å thermally-grown SiO<sub>2</sub> layer was deposited by furnace. After the SiO<sub>2</sub> deposition, we try to remove the SiO<sub>2</sub> layer from the wafer of unpolished-side. The etching-solution we used is buffered oxide etching (B.O.E.) solution (40% NH<sub>4</sub>F and 1 part 49% HF). Hence, the wafer of unpolished-side without SiO<sub>2</sub> layer can serve as a gate-electrode. Finally, the substrate was cleaned in ultrasonic tank by the sequence of: de-ionic water (5 minutes), acetone (1 minutes), and de-ionic water (5 minutes).



### 3-1-3 Surface Treatment

After substrate cleaning, we dip the octadecyltrimethoxysilane (ODMS) and 3-Aminopropyltriethoxysilane (APTES) individually unto the substrate. Consequently, we try to remove the residual solvent. The substrates are then baked in the oven at 120°C about 15 minutes.

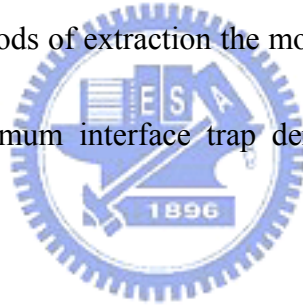
### 3-1-4 Growth of Thin Film and Electrodes

Pentacene, which was obtained from Aldrich Chemical Company without any purification, was used as an active layer. The deposition is started at a pressure lower than  $3 \times 10^{-6}$  torr. The deposition rate is controlled at 0.5Å/s. The temperature we use in

depositing pentacene films is 70 °C. All the deposition parameters are monitored by a quartz crystal microbalance (QCM) during the deposition process. In the end, a 1000Å Au layer was used as the source and drain pad, which is deposited at a rate of 1 Å/sec under  $3 \times 10^{-6}$  torr. The channel width (W) and length (L) defined by shadow-mask was 800µm and 1200µm, respectively. Finally, the device is shown in Fig. 3.2.

### 3-2 Measurement Methods and Parameter Extraction

In this section, the methods of extraction the mobility, the threshold voltage, the subthreshold swing, the maximum interface trap density, and the is characterized, respectively.



#### 3-2-1 Mobility

Generally, the linear mobility (for  $V_D < V_G - V_{th}$ ) can be extracted from the transconductance maximum  $g_m$  in the linear region:

$$g_m = \left[ \frac{\partial I_D}{\partial V_G} \right]_{V_D = \text{const}} = \frac{WC_{ox}}{L} \mu V_D \quad (2.5)$$

The saturation mobility (for  $V_D > V_G - V_{th}$ ) can also be extracted from the slope of the curve in the squared drain-current versus the gate-voltage diagram:

$$\sqrt{I_D} = \sqrt{\frac{W}{2L} \mu C_{ox} (V_G - V_{TH})} \quad (2.6)$$

### 3-2-2 Threshold voltage

We extract the threshold voltage from equation (2.6), the intersection point of the squared drain-current versus gate-voltage.

### 3-2-3 Subthreshold swing

Subthreshold swing is also important characteristics for device application. It is a factor to estimate how rapidly the device switches from the off state to the on state in the region of exponential current increase. It is defined by:

$$S = \left. \frac{\partial V_G}{\partial (\log I_D)} \right|_{V_D = \text{constant}}, \text{ when } V_G < V_T \text{ for p-type.}$$

Moverover, the subthreshold swing also represents the interface quality and the defect density [2], the maximum interface state trap-density can be extracted by :

$$N_{ss} = \left[ \frac{S \cdot \log(e)}{kT/q} - 1 \right] \cdot \frac{C_i}{q}$$

A high-performance TFTs will show a lower subthreshold swing.

### 3-2-4 On/Off current ratio

Devices with high on/off current ratio represent large turn-on current and small off current. It determines the gray-level switching of the displays. High on/off

current ratio means there are enough turn-on current to drive the pixel and sufficiently low off current to keep in low power consumption.

### 3-3 Gas-Sensing system

As shown in Fig. 3.3, the gas-sensing system consists of three major parts: a gaseous analyte controller, a gas-proof chamber, and a semiconductor parameter analyzer. In Fig. 3.4(a), (b), and (c), we show the mass flow controller, the power supply, and pressure gauge, respectively. The gaseous analyte was introduced into the gas-proof chamber via the mass flow controllers (MFC; 5850E, Brooks Instrument). The pressure inside the gas-proof chamber is monitored by vacuum gauge (PC-615). The total volume of the gas-proof chamber is about 40 liter. Fig. 3.5 is the top-view image of gas-sensing system. The system is equipped with five Kelvin-probes and positioners. The probes were connected to the semiconductor analyzer (Keithley 4200-SCS&2636) via tri-axial cables. The bottom pipe and the upper pipe serve as the gas-inlet and gas-exhaust, respectively. After mounting a metal cap with transparent window, the gas-proof chamber can be pumped down to less than 1 torr. Consequently, we introduce the pure nitrogen gas into the gas-proof chamber. Thus, all the gaseous-sensing experiments can be processed in a low-humidity and low-oxygen ambiance. All the experiments were also be operated at a pressure about 760 torr.

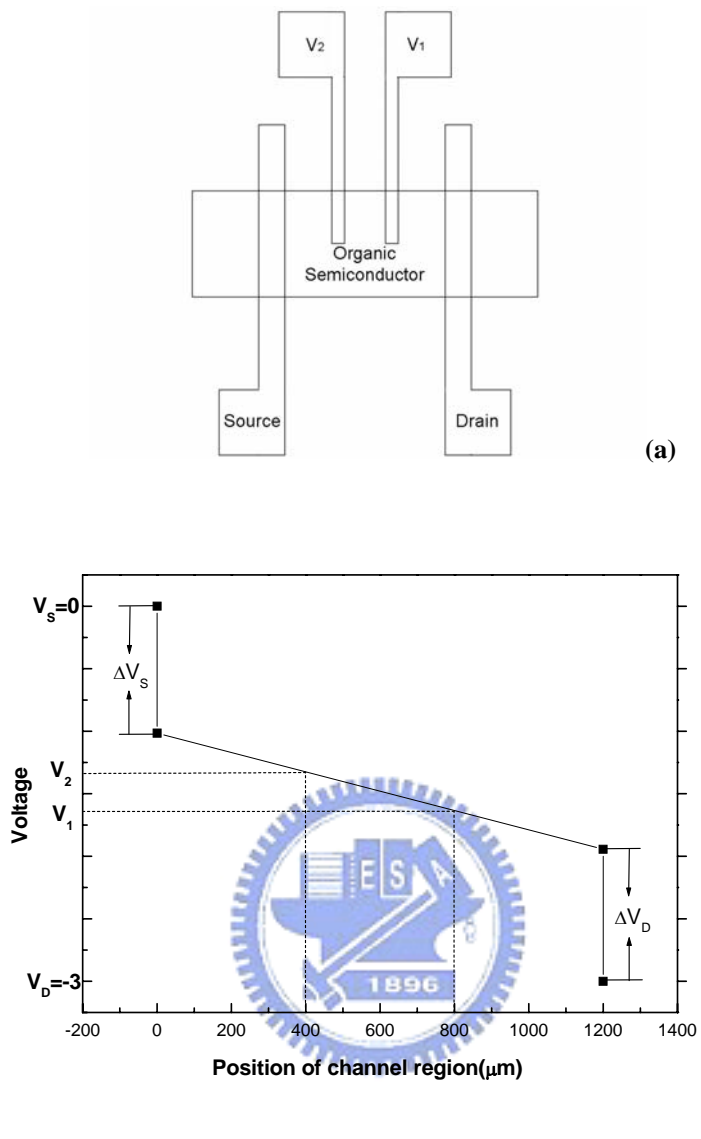


**Figure 3.1.** (a) Top view of a field-effect device. (b) Schematic voltage drop along the channel for an OTFT biased in the linear region of device operation. The potential drop between the voltage-probing electrodes is assumed to be linear for the evaluation of the mobility from the four-terminal measurement.

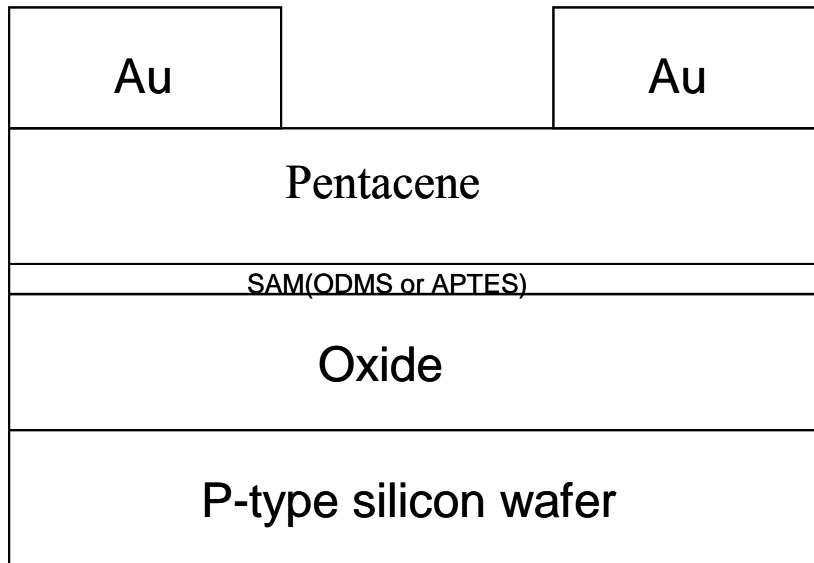


**Fig.3.2** The device structure of SAM-treated OTFTs.

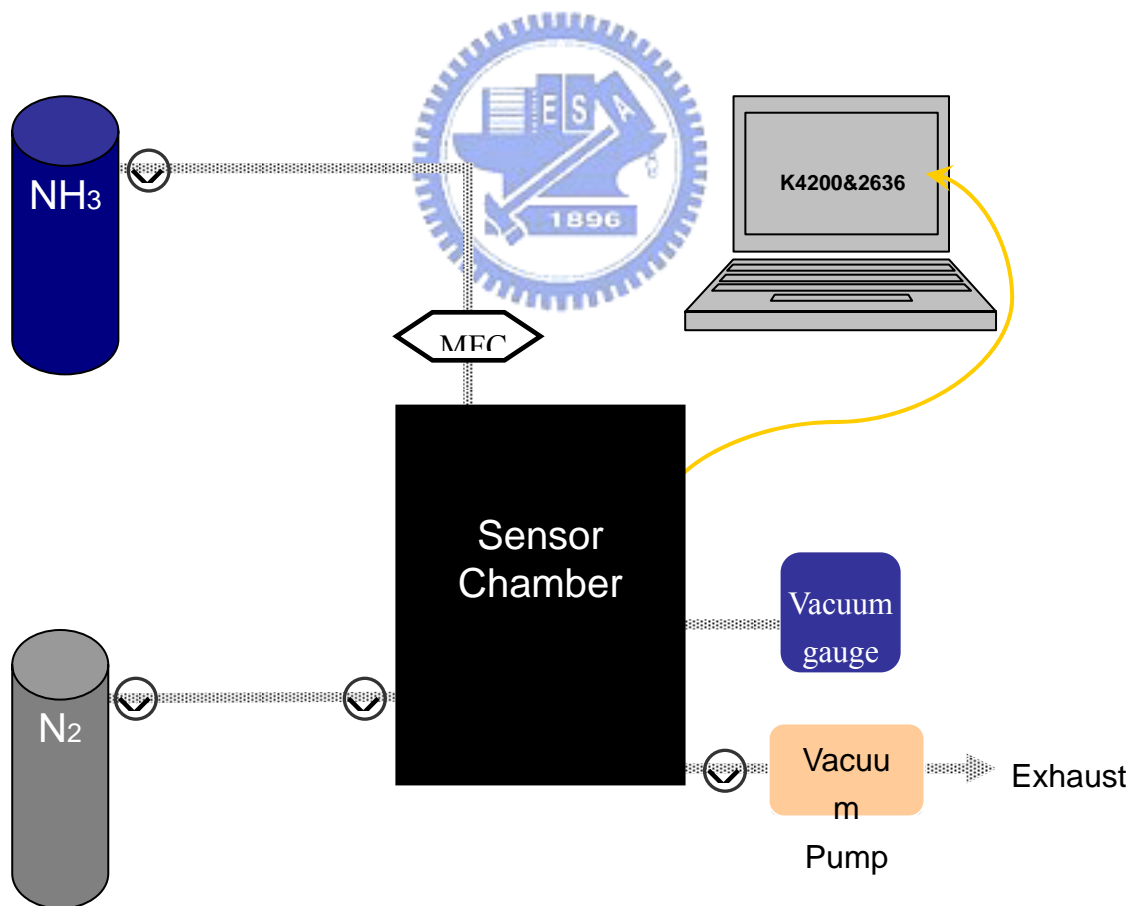
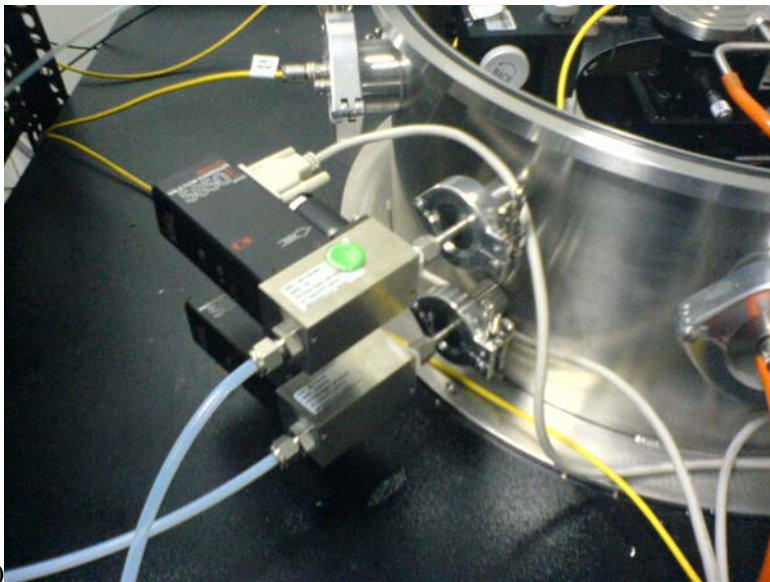


**Figure 3.3** sensor measurement system.





(a)



(b)

**Figure 3.4** analyte control system.

- (a) There is a four channel Mass Flow Controller (MFC) Readout Power Supply, and a vacuum gauge.
- (b) There is a Mass Flow Controller

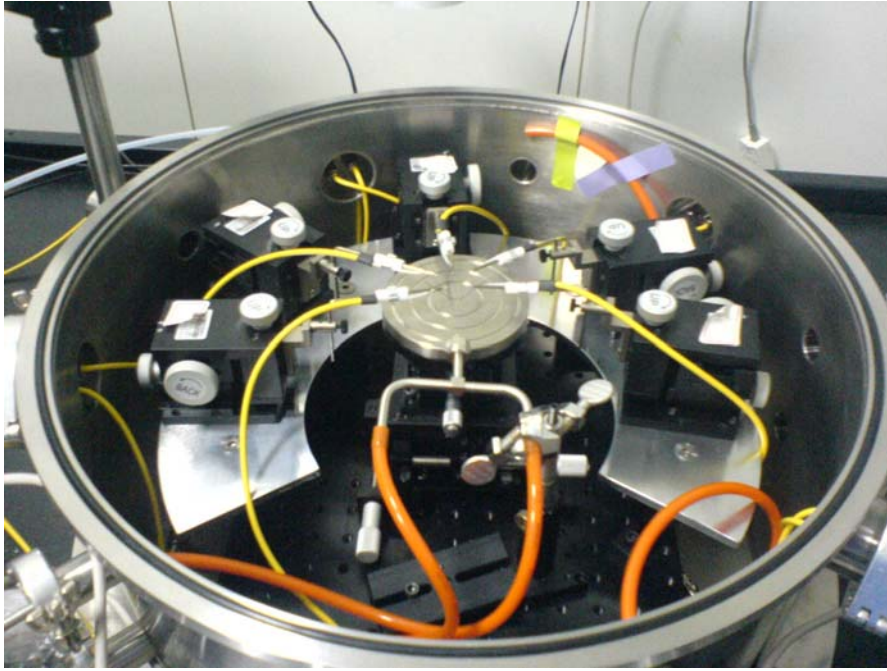


**Figure 3.5** Chamber used for sensor experiments.



# Chapter 4

## Experiments Results and Discussion

### 4-1 SAM with APTES/ODMS

#### 4-1-1 Percentage Control

Before identifying quality of SAM including ODMS and APTES, we try to mix ODMS and APTES. First, we must find the solvent including ethanol to dissolve ODMS and APTES. We observe that ethanol can dissolve both ODMS and APTES, but the sample must be overnight after dipping. Then, we change percentage of ODMS mixed APTES and the percentage are 100%ODMS, 90%ODMS/10%APTES, 50%ODMS/50%APTES, and 100%APTES, respectively. And, the percentage is volume ratio for ODMS and APTES.

#### 4-1-2 Molecule Immobilization

The quality of ODMS and APTES immobilization can be approved by SEM, AFM, anti-body, and protein immobilization. The amine groups ( $-NH_2$ ) of APTES can covalent bonding with anti-body, and anti-body is big molecular which has 10nm Au atom on the end so we can use SEM to check the growth condition of APTES. The result was shown in the inset of Fig. 4.2(a). In Fig. 4.2(a), we observe that Au atoms exist and the size of Au atom is about 10nm. But, the quantity of Au atom is too less so this method using SEM to check existence of BSA isn't better.

Then, we use AFM to check the existence of BSA in Fig. 4.2(b). In Fig. 4.2(b), we deduced that protein truly draws in by APTES and not by ODMS. Besides, protein

on APTES is uniform and there is no protein on ODMS because there is no functional group on ODMS to covalent bond with BSA. We also deduced APTES truly grow on SiO<sub>2</sub> because of AFM of BSA covalent bonded with APTES. Finally, we conclude that the method of AFM of BSA can be observed more easily than the method of SEM of BSA.

## **4-2 Material and electrical analysis on SAM-OTFTs**

### **4-2-1 AFM analysis of SAM quality**

By ODMS, ODMS mixed with APTES and APTES-dipped SiO<sub>2</sub>, we try to initiate surface characteristics of SAM. In Fig. 4.2(b), we show the atomic force microscope (AFM) images of ODMS and APTES treated SiO<sub>2</sub> dielectric. In the Table III, as we can observe, we proposed ODMS, ODMS mixed with APTES, APTES and the surface roughness of ODMS, ODMS mixed with APTES including ODMS/APTES=90%/10% and 50%/50%, APTES-dipped SiO<sub>2</sub> are about 0.234nm, 0.356nm, 0.369nm, and 0.221nm, respectively. APTES and ODMS have different numbers of carbon chain so the length of carbon chains between ODMS and APTES are different. We deduced the roughness of ODMS mixed APTES is bigger because the length of carbon chains between ODMS and APTES are different, and ODMS and APTES can't match well to induce to broken bonds. Then we choose ODMS and APTES as our SAM in after research because ODMS mixed APTES-dipped SiO<sub>2</sub> is

too rough. Additionally, we also understand that the ODMS and APTES will not affect the surface roughness of SiO<sub>2</sub> significantly, so pentacene can grow on ODMS and APTES treated SiO<sub>2</sub> well. The AFM image of pentacene on SAM-dipped SiO<sub>2</sub> layer is also show in Fig. 4.2(c).It seems that the grain of pentacene on ODMS treated SiO<sub>2</sub> is bigger than that on APTES treated SiO<sub>2</sub> because of surface energy difference between ODMS and APTES treated SiO<sub>2</sub>.

#### **4-2-2 Electrical Characteristics of OTFTs with distinct SAM-dielectrics**

Before ammonia is introduced into chamber, we compare electrical characteristics of ODMS and APTES-OTFTs including threshold voltage, mobility, and Subthreshold swing. After the source (Au), drain (Au), and voltage-probing electrodes are deposited on pentacene film, we measured the transfer characteristics of the gated-4-probes OTFT. The drain-current is plotted as a function of gate-voltage in Fig. 4.3. When gate bias changes from 5V to -50V and drain bias is -3V, the devices shows an on/off current ratio about 4 order for APTES-OTFTs and about 6 order for ODMS-OTFTs but the  $I_{on} \sim 10^{-7} A$  for ODMS and APTES-OTFTs are the same.

It also shows threshold voltage difference for ODMS and APTES-OTFT from -11.75 V to -43.6 V. The  $V_{th}$  difference may be attributing to  $-NH_2$  on APTES because of the negative charge of  $-NH_2$  to trap the main carrier-hole. Mobility for ODMS and APTES-OTFTs are 0.33 and 0.038 cm<sup>2</sup>/Vs, respectively. The difference of mobility

between ODMS and APTES-OTFTs may be  $-\text{NH}_2$  on APTES to trap hole carriers. Subthreshold swing for ODMS and APTES-OTFTs are 1.34 and 1.73 V/decade, respectively. The Electrical Characteristics results show in the Table IV. We deduced  $-\text{NH}_2$  on APTES will trap hole and induced that the threshold voltage will shift more negatively, on current, and mobility will get smaller, but it doesn't affect Subthreshold swing a lot.

### **4-3 Effects of ammonia ( $\text{NH}_3$ ) on Gated four-probe OTFTs**

#### **4-3-1 Id-Vg curve variation**

Before the measurement, the gas-sensing chamber is pumped-down to less than 1 torr and vented to 760 torr by the high-purity nitrogen ( $\text{N}_2$ ) gas. Initially, we measured the gated-4-probe OTFT in the nitrogen ambience. Before ammonia ( $\text{NH}_3$ ) is introduced into the chamber, we expected that ODMS and APTES-OTFTs are different in the change of threshold voltage shift and change of mobility because there is  $-\text{NH}_2$  on APTES and will be expected not to react with  $\text{NH}_3$ . First, we analysis the id-Vg curve of ODMS and APTES-OTFT in 5mins, 10mins and 20mins in the 0.5ppm ammonia, and change gate bias from 5V to -45V and drain bias is fixed in -3V. We expect to observe that mobility and threshold voltage will saturate. The electrical characteristics of ODMS and APTES-OTFT are shown in Fig. 4.4(a) and 4.4(b). When the  $\text{NH}_3$  is introduced into the chamber, the drain-current ( $I_D$ ) will reduced

from 5mins to 20mins. Interestingly, the threshold voltage will also shift more negatively, and field-effect mobility will decrease. But, we observe that the threshold voltage and mobility will saturate in 10mins in Fig. 4.5(a) and 4.5(b). So we decide to choose 10mins as our main parameter in our next experiment.

Then, we change the quantity of ammonia ( $\text{NH}_3$ ) from 0.5ppm to 1.5ppm. And, we also change gate bias from 0V to -50V and drain bias is fixed in -3V. Then we measured the drain-current plotted as a function of gate-voltage every 10mins as the quantity of  $\text{NH}_3$  is 0.5ppm, 1ppm, 1.5ppm. In Fig. 4.6(a) and 4.6(b), when the  $\text{NH}_3$  is introduced into the chamber, the drain-current ( $I_D$ ) will reduced with the increase of the  $\text{NH}_3$  concentration in Fig. 4.6(c). The decrease of on current is because of mobility or threshold voltage change by 2.6. In 4.3.3, we will analysis mobility and threshold voltage change with the increase of the  $\text{NH}_3$  concentration. Interestingly, the threshold voltage will also shift more negatively, and field-effect mobility will decrease with the increase of the  $\text{NH}_3$  concentration. The on/off current ratio and the subthreshold swing will not be changed significantly with the increase of the  $\text{NH}_3$  concentration.

#### **4-3-2 Contact resistance variation**

To further study the effects of  $\text{NH}_3$  gas on OTFT devices, we try to estimate the

contact resistance and pentacene resistance by the gated-4-probe OTFT, respectively.

From potential-probes on channel, the voltage-drops at the source electrode ( $\Delta V_S$ ),

drain electrode ( $\Delta V_D$ ), and within the pentacene film ( $\Delta V_{film}$ ) can be estimated by:

$$\Delta V_S = [V_1 - \frac{(V_2 - V_1)}{(L_2 - L_1)} \cdot L_1] - V_S$$

$$\Delta V_D = V_D - [V_2 + \frac{(V_2 - V_1)}{(L_2 - L_1)} \cdot (L - L_2)]$$

$$\Delta V_{film} = \frac{(V_2 - V_1)}{(L_2 - L_1)} \cdot L$$

$V_1$  and  $V_2$  is the voltage measured from the first potential probe (near the source electrode) and second potential probe (near the drain electrode), respectively.  $L_1$

and  $L_2$  is the distance from the first potential probe to source electrode and the second potential probe to drain electrode.  $L$  is the channel length.  $V_D$  and  $V_S$  is the drain voltage and source voltage, respectively.

The total contact resistance ( $R_{cont}$ )

and film resistance ( $R_{film}$ ) can also be estimate by:

$$R_{cont} = \frac{\Delta V_S + \Delta V_D}{I_D}$$

$$R_{film} = \frac{\Delta V_{film}}{I_D}$$

As shown in Fig. 4.7, the  $R_{cont}$  and  $R_{film}$  is plotted as a function of gate-voltage



minus threshold-voltage ( $V_G - V_{th}$ ), respectively. The  $R_{cont}$  and  $R_{film}$  get smaller with more minus  $V_G - V_{th}$  and get smaller as the quantity of  $NH_3$  get much more for ODMS-OTFTs but get bigger for APTES-OTFTs. The Fig. 4.8(a) and 4.8(b) shows the percentage (%) of  $R_{cont}$  and  $R_{film}$  versus injected  $NH_3$ , respectively. It is clear that the percentage (%) of  $R_{film}$  is as high as about 90% during the  $NH_3$  gaseous experiment for ODMS and APTES-OTFTs. Thus, the OTFT characteristics should be mainly dominated by the pentacene film properties rather than the contact properties.



#### 4-3-3 Threshold voltage and mobility variation

Since the pentacene film properties will dominate the OTFT characteristics during the  $NH_3$  gaseous experiment, we try to observe the intrinsic variation of field-effect mobility. In gated-4-probes measurement, the contact-corrected field-effect mobility ( $\mu_{eff}$ ) can be extracted by

$$\mu_{eff} = \frac{1}{C_{total}} \cdot \frac{\partial \sigma}{\partial V_G}$$

$$\sigma = \frac{I_D}{V_2 - V_1} \cdot \frac{L'}{W}$$

where  $C_{total}$  is the total capacitance of OTFT,  $\sigma$  is the conductivity,  $V_1$  and  $V_2$  is the voltage measured from the first potential probe (near the source electrode) and second potential probe (near the drain electrode),  $L'$  is the distance between two

potential probes, and  $W$  is the channel width.

The threshold voltage shift ( $\Delta V_{th}$ ), intrinsic field-effect mobility, and the subthreshold swing ( $S.S.$ ) is also plotted as a function of  $NH_3$  concentration in Fig. 4.9 and Fig. 4.10, Fig.4.11, respectively. In Fig. 4.9, the threshold voltage will shift toward more negatively from -11.75V to -19.94V for ODMS-OTFTs and from -43.6V to -50.34V for APTES-OTFTs with the increase of  $NH_3$  concentration. But for ODMS-OTFTs, the change of threshold voltage ( $V_{th}$  %) is bigger than that of APTES-OTFTs. The reason might be  $-NH_2$  on APTES don't react with  $NH_3$  dramatically and repel  $NH_3$  so there is less  $NH_3$  to trap carrier that  $V_{th}$  % is smaller for APTES-OTFTs than ODMS-OTFTs. In Fig. 4.10, the field-effect mobility will decrease from 0.33  $cm^2/Vs$  to 0.314  $cm^2/Vs$  with the increase of  $NH_3$  concentration for ODMS-OTFTs and from 0.038  $cm^2/Vs$  to 0.029  $cm^2/Vs$  for APTES-OTFTs. But for ODMS-OTFTs, the change of field-effect mobility ( $\mu$  %) is smaller than that of APTES-OTFTs. However, the subthreshold swing is kept at an averaged value around  $1.28 \pm 0.05V/decade$  and  $1.76 \pm 0.09V/decade$  for ODMS and APTES-OTFTs, respectively, and seems not to be affected by the  $NH_3$  dramatically, even when the  $NH_3$  concentration is approached to a concentration of 1.5ppm. Finally, we deduced that the difference of the change of threshold voltage ( $V_{th}$  %), field-effect mobility ( $\mu$  %) between ODMS and APTES-OTFTs may be because of  $-NH_2$  on APTES but no

functional group on ODMS.

In Fig. 4.12, we observe that when the  $\text{NH}_3$  molecular is introduced, the molecular will be adsorbed by the pentacene film. The polycrystalline pentacene with a lot of GBs will serve additional sites to interact with  $\text{NH}_3$  molecular. Hence, the absorbed  $\text{NH}_3$  molecular on the GBs will increase the barrier height and acts as trapping sites ( $Q_{\text{trap}}$ ). In our experiment, an increased (negatively shift) threshold voltage implies the concentration of mobile holes in the pentacene film will be reduced. But for APTES-OTFTs, there are functional groups ( $-\text{NH}_2$ ) to repel  $\text{NH}_3$  molecular and  $Q_{\text{trap}}$  is less so the quantity of threshold voltage shift is smaller in Fig. 4.9. We also observe that the quantity of the change of intrinsic field-effect mobility for APTES-OTFTs is bigger than ODMS-OTFTs in Fig. 4.10. Because the grain boundaries of pentacene on APTES are more than those on ODMS, more GBs will absorb more  $\text{NH}_3$  molecular to affect carrier conduction. And, we deduced the change of maximum on current by comparing the change of mobility and threshold voltage in Fig. 4.6(c). By 2.6, we understand that the change of maximum on current ( $\Delta I_{\text{on}}$ ) is smaller for APTES-OTFTs because the change of mobility is bigger and the change of threshold voltage is smaller. Finally, we understand that the quantity of GBs affects the change of mobility, the quantity of  $Q_{\text{trap}}$  affects the threshold voltage shift, and the change of mobility and the threshold voltage shift influence  $\Delta I_{\text{on}}$ .

**Table II** The surface roughness of ODMS, ODMS mixed with APTES, APTES-dipped SiO<sub>2</sub>

|                | <b>ODMS</b>  | <b>ODMS/APT<br/>ES=90%/10<br/>%</b> | <b>ODMS/APT<br/>ES=50%/50<br/>%</b> | <b>APTES</b> |
|----------------|--------------|-------------------------------------|-------------------------------------|--------------|
| <b>Rms(nm)</b> | <b>0.234</b> | <b>0.356</b>                        | <b>0.369</b>                        | <b>0.221</b> |

**Table III** The comparison of ODMS and APTES -OTFTs electrical properties

| <b>Treated</b>     | $\mu(cm^2/Vs)$ | $V_{th}(V)$   | <b>Subthreshold<br/>swing(V/decade)</b> | <b>on/off ratio</b>        |
|--------------------|----------------|---------------|---|----------------------------|
| <b>ODMS-OTFTs</b>  | <b>0.33</b>    | <b>-11.75</b> | <b>1.34</b>                             | <b>&gt; 10<sup>6</sup></b> |
| <b>APTES-OTFTs</b> | <b>0.038</b>   | <b>-43.6</b>  | <b>1.73</b>                             | <b>&gt; 10<sup>4</sup></b> |

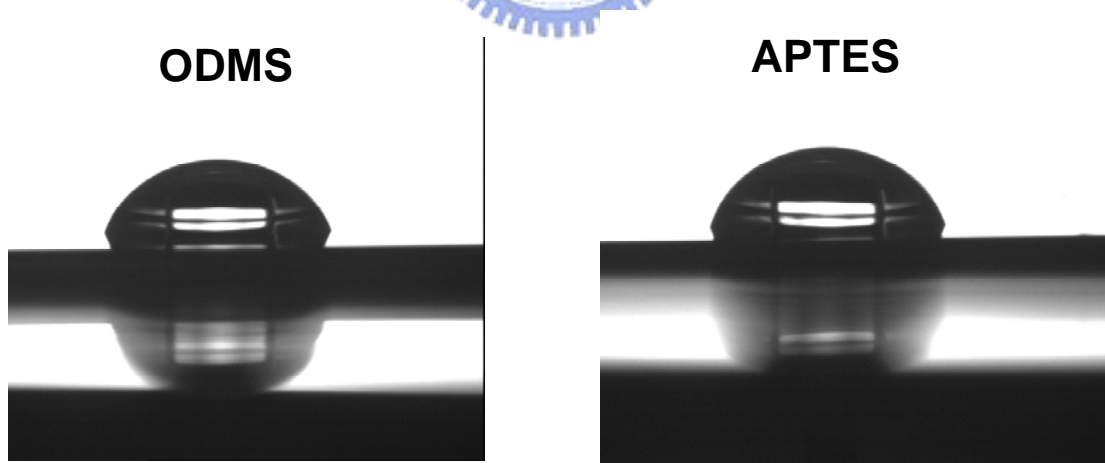


**Fig. 4.1** The contact angle of the de-ionized water on ODMS-treated SiO<sub>2</sub> surface, and on APTES-treated SiO<sub>2</sub> surface, respectively.

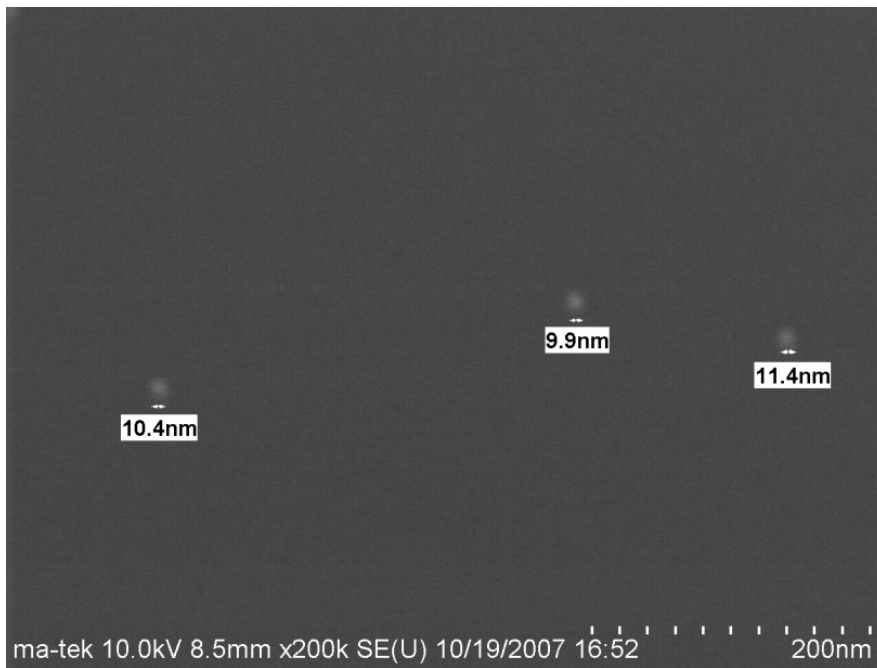


**Fig. 4.2(a)** The amine groups of APTES can covalent bonding with anti-body.

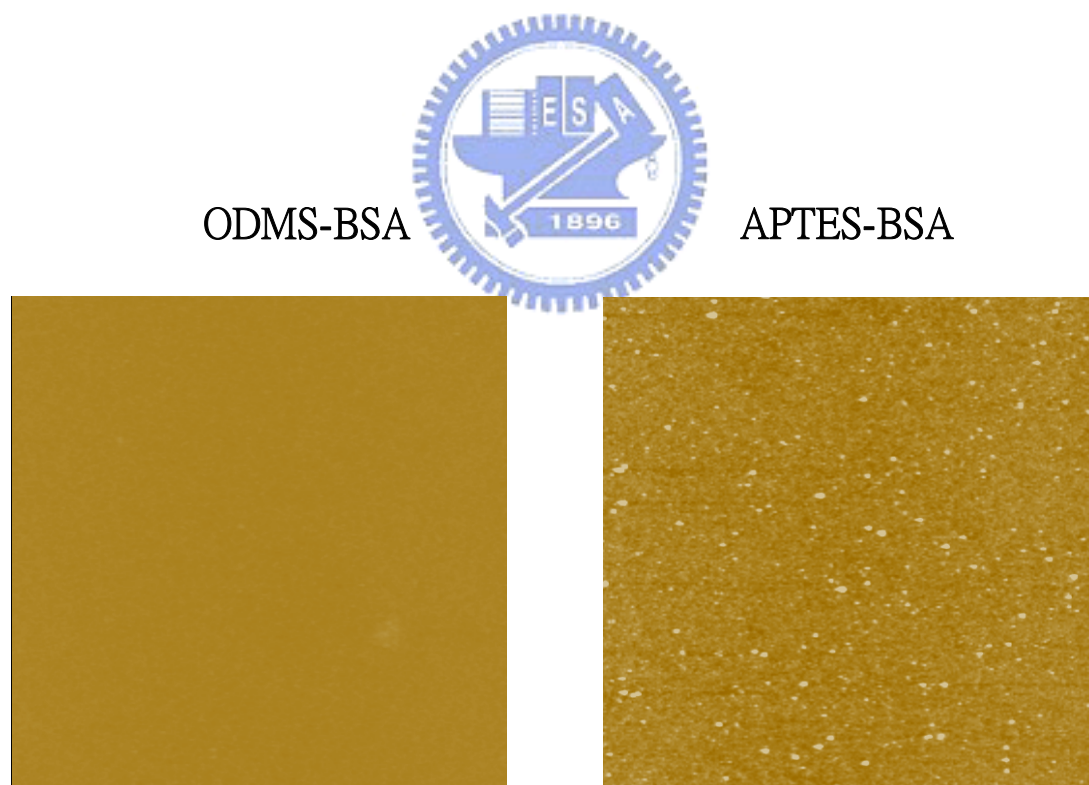
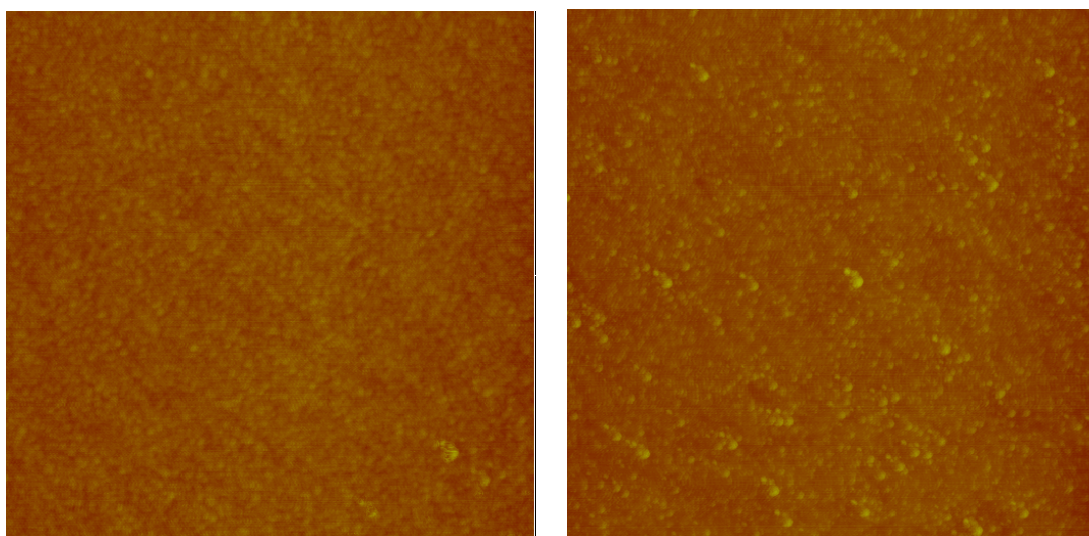


**Fig. 4.2(b)** The amine groups of APTES can covalent bonding with bovine serum albumin (BSA). And BSA is shown in the AFM.



**ODMS**

**APTES**

**Fig. 4.2(c)** atomic force microscope (AFM) images of SAM-dipped SiO<sub>2</sub> dielectric for ODMS and APTES

**ODMS-pentacene**

**APTES-pentacene**

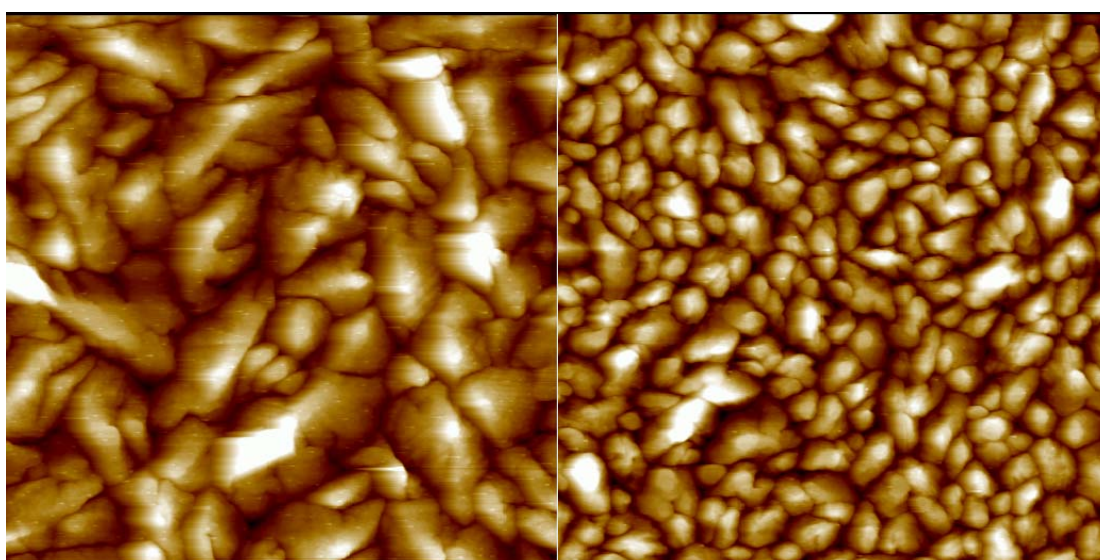


**Fig. 4.2(d)** pentacene AFM image on SAM-dipped SiO<sub>2</sub> layer for ODMS and APTES

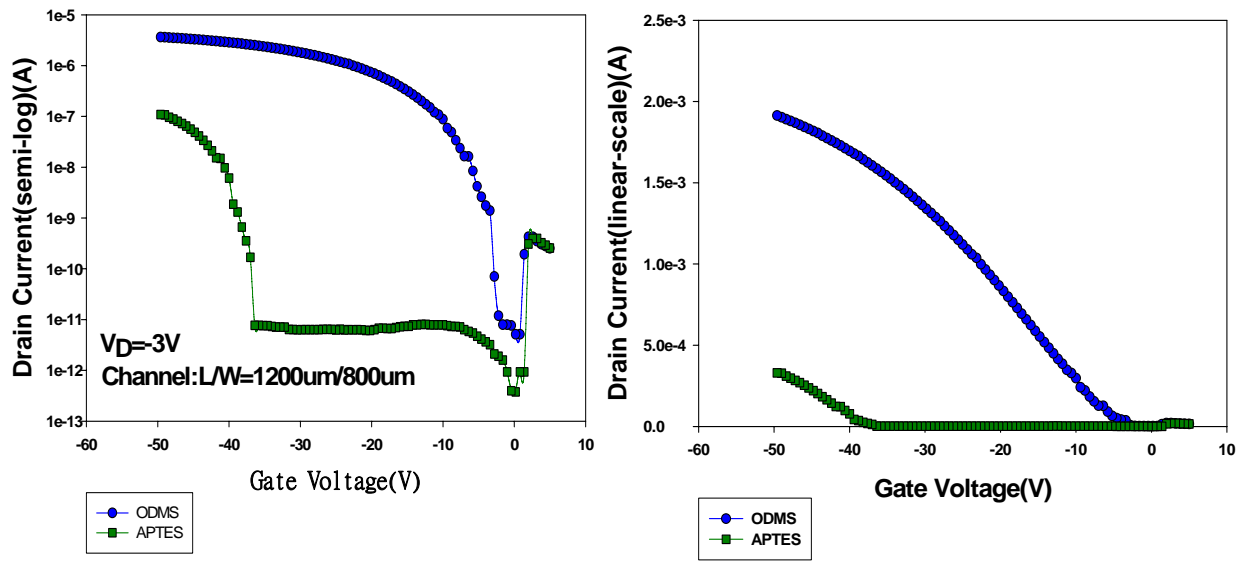


**Fig. 4.3** Transfer characteristics of OTFT with treated ODMS/APTES dielectric



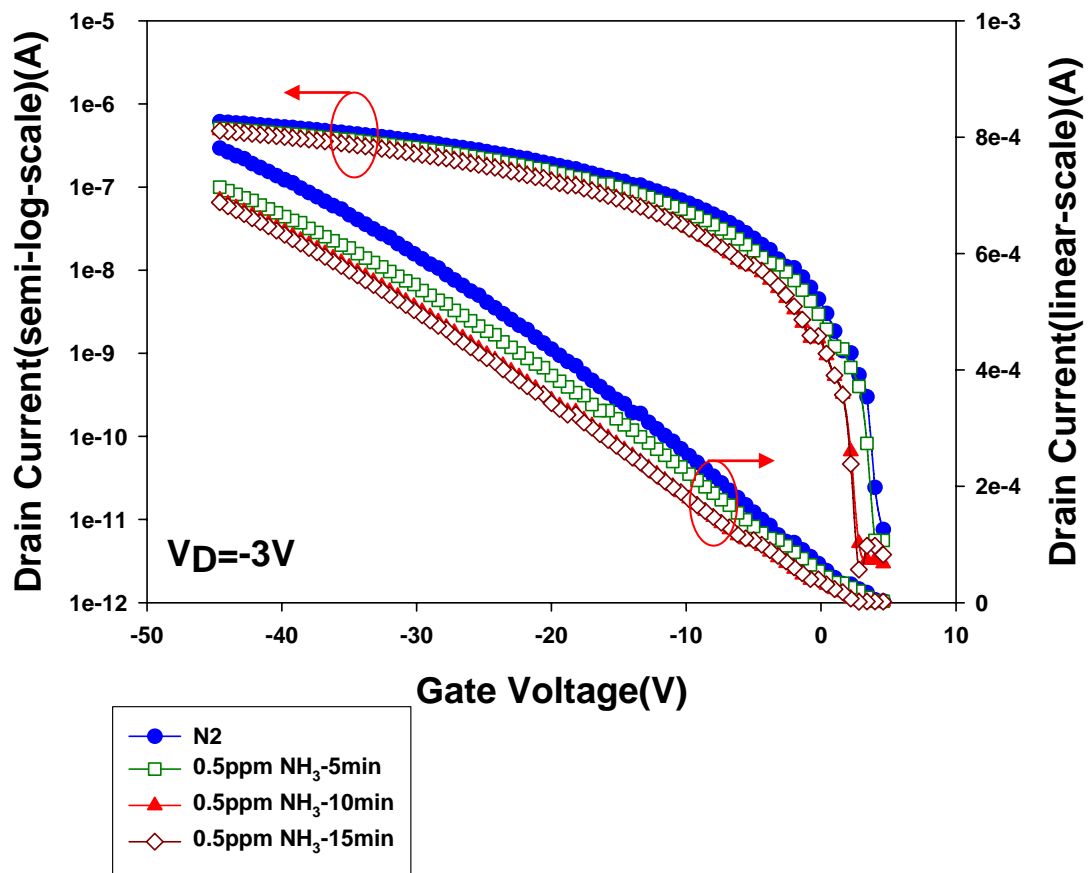


**Fig.4.4 (a)** Electrical characteristics of ODMS-OTFTs in 0.5ppm NH<sub>3</sub> in 5mins, 10mins, and 20mins.



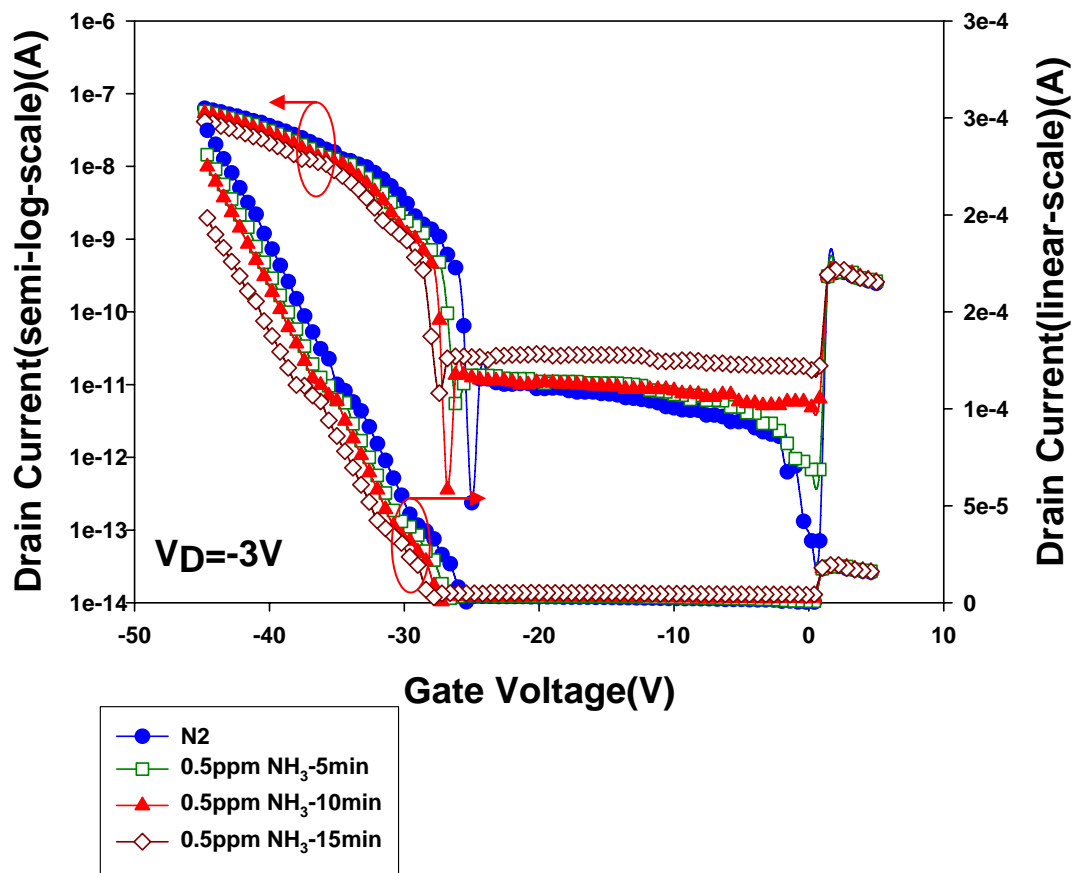


**Fig.4.4 (b)** Electrical characteristics of APTES-OTFTs in 0.5ppm NH<sub>3</sub> in 5mins, 10mins, and 20mins.

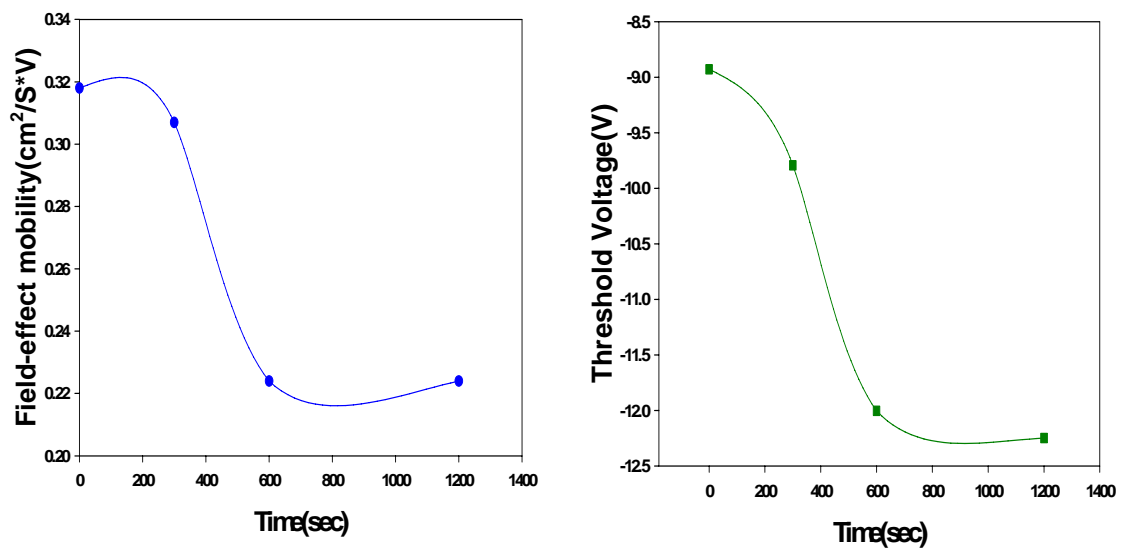


**Fig.4.5(a)** field-effect mobility and threshold voltage of ODMS-OTFTs in 0.5ppm NH<sub>3</sub> in 5 mins, 10mins, and 20mins.

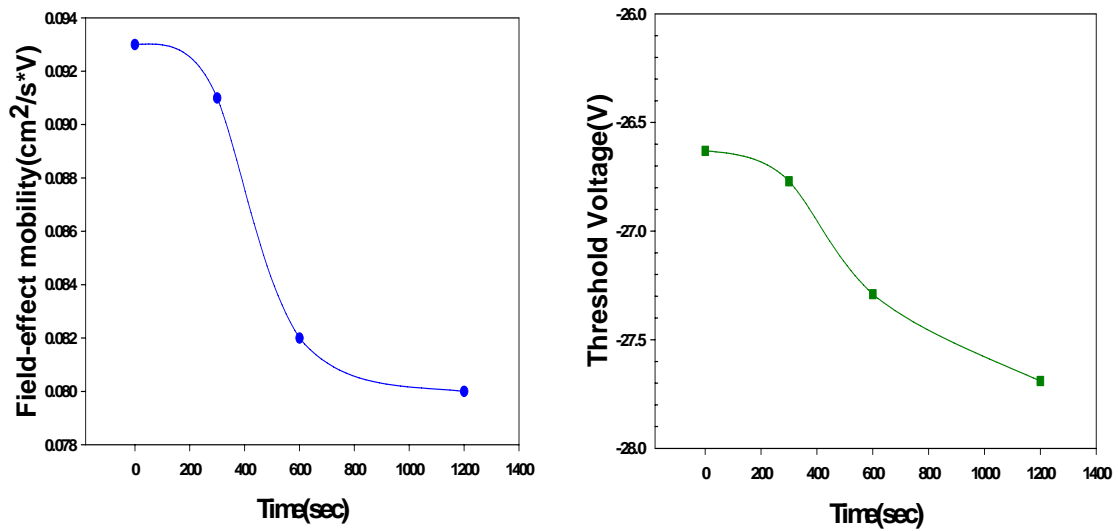


**Fig.4.5(b)** field-effect mobility and threshold voltage of APTES-OTFTs in 0.5ppm NH<sub>3</sub> in 5 mins, 10mins, and 20mins.

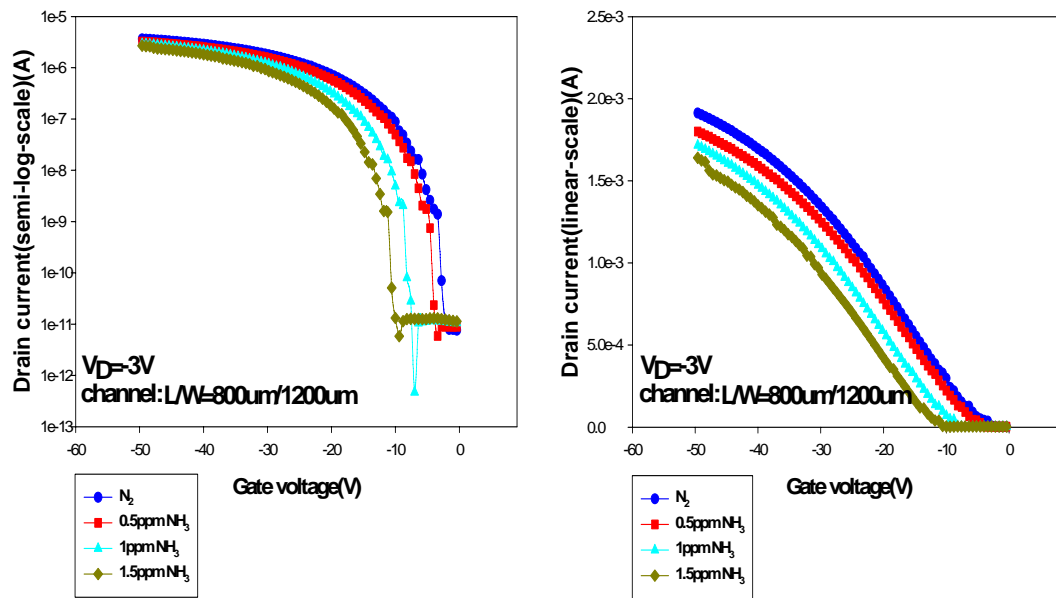


**Fig.4.6(a)** Electrical characteristics of ODMS-OTFTs in NH<sub>3</sub>.

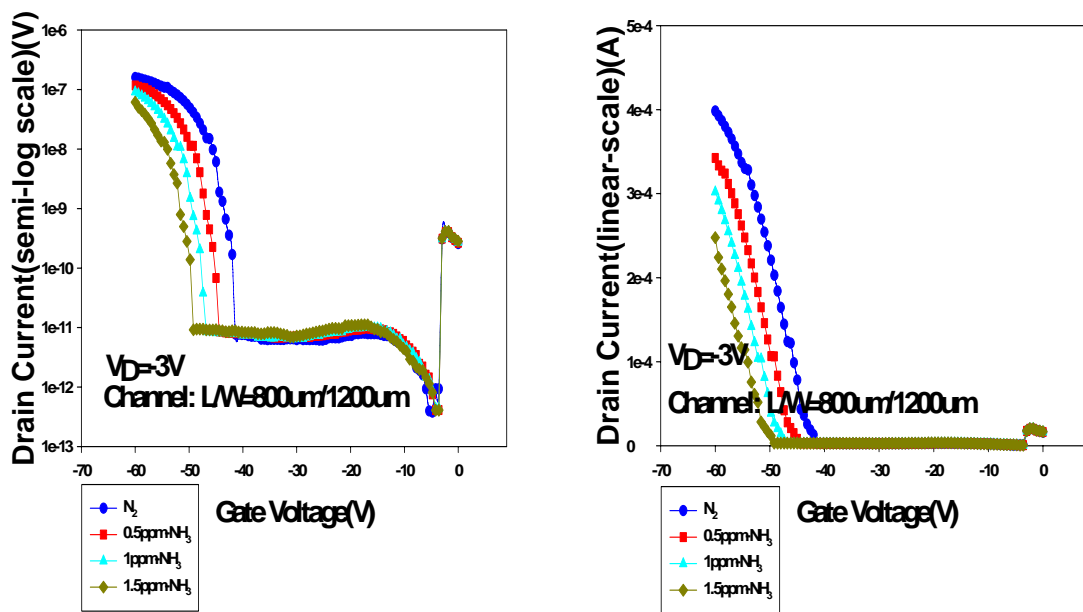


Fig.4.6(b) Electrical characteristics of APTES-OTFTs in NH<sub>3</sub>.

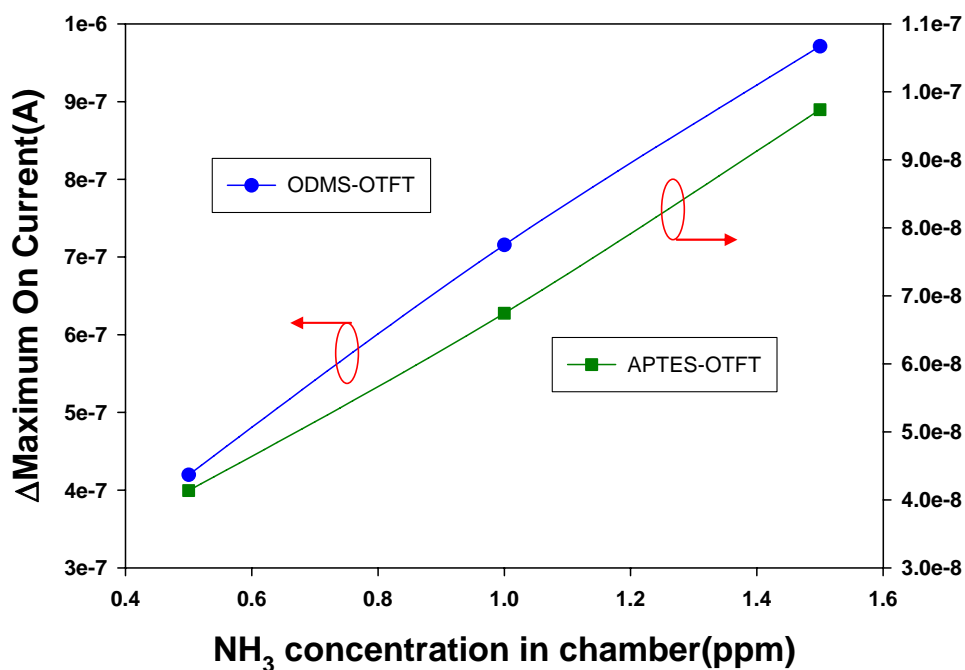


Fig. 4.6(c) the change of maximum on drain-current ( $I_D$ ) of ODMS and APTES-OTFT versus NH<sub>3</sub> concentration

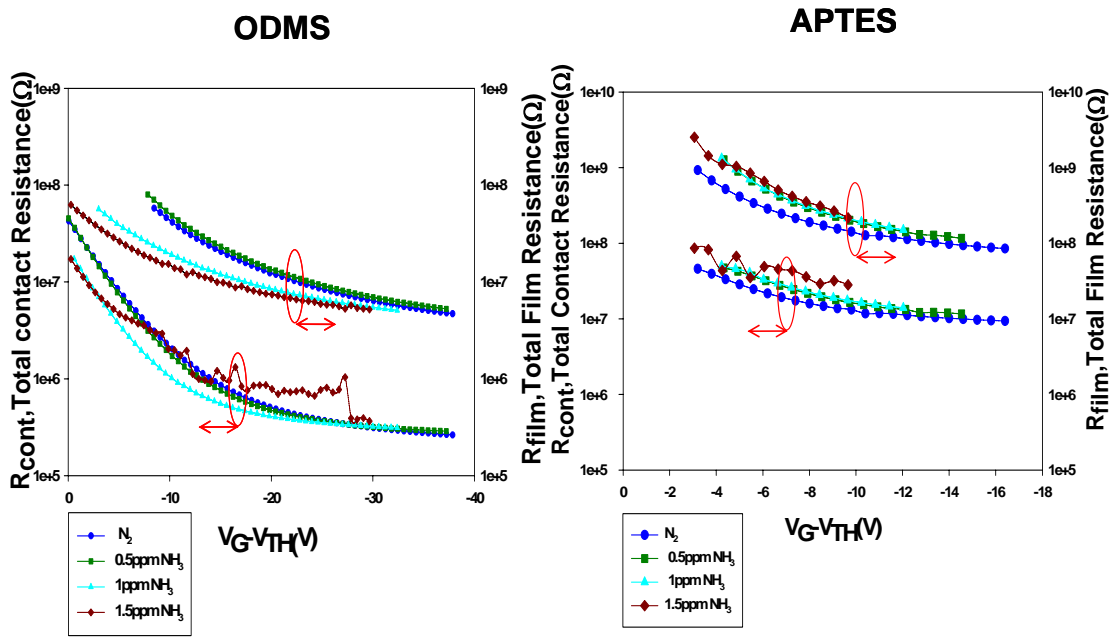


Fig. 4.7 The  $R_{cont}$  and  $R_{film}$  are plotted as a function of gate-voltage minus threshold-voltage ( $V_G - V_{th}$ ), respectively.

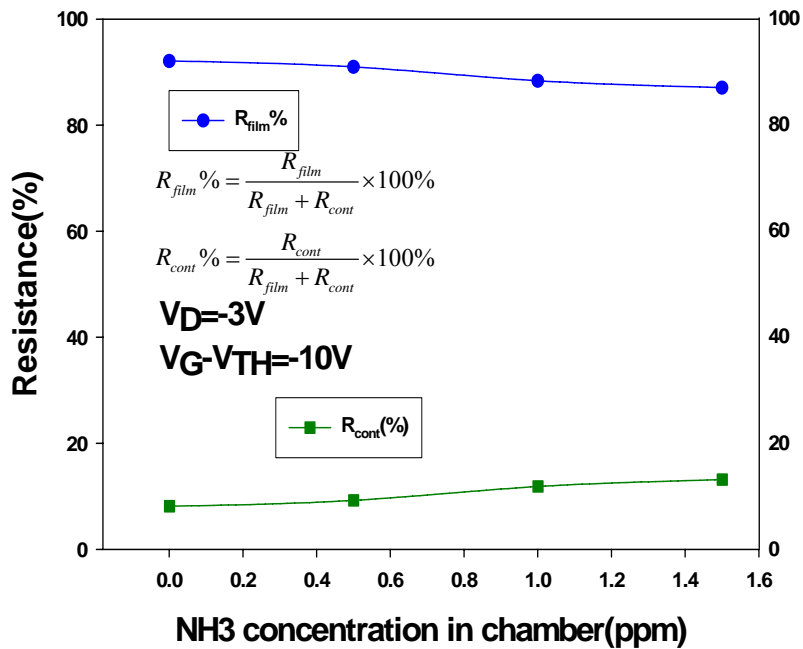


Fig. 4.8(a) For ODMS-OTFTs, the percentage (%) of  $R_{cont}$  and  $R_{film}$  versus injected  $NH_3$ .

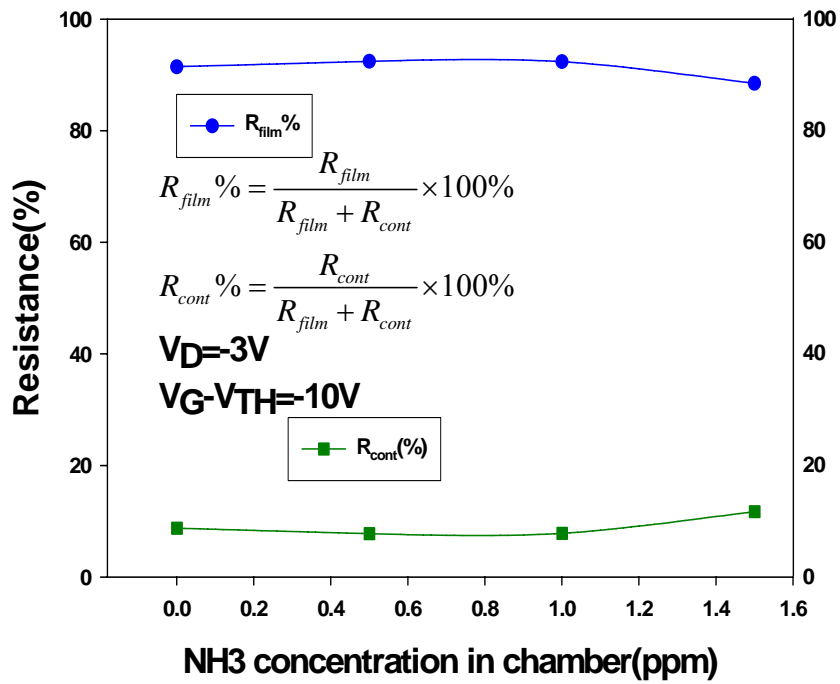


Fig. 4.8(b) For APTES-OTFTs, the percentage (%) of  $R_{cont}$  and  $R_{film}$  versus injected NH<sub>3</sub>.

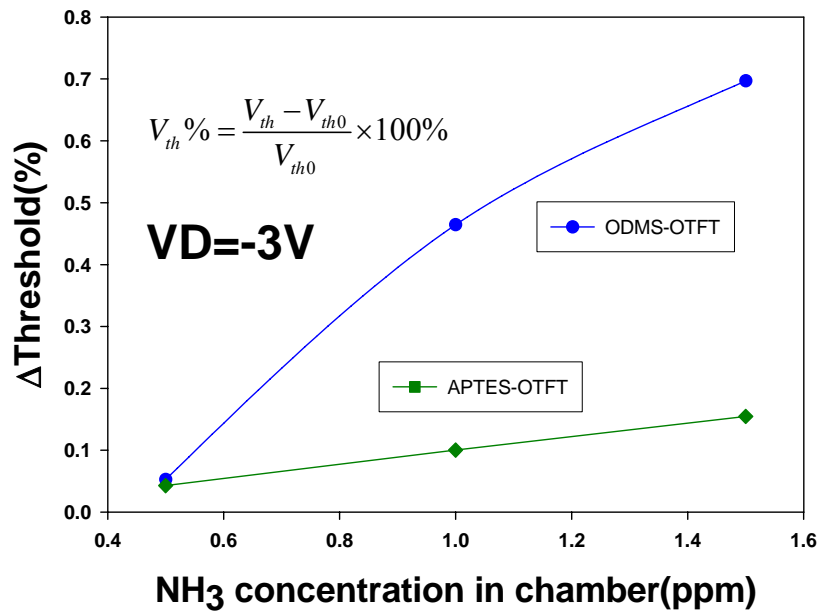
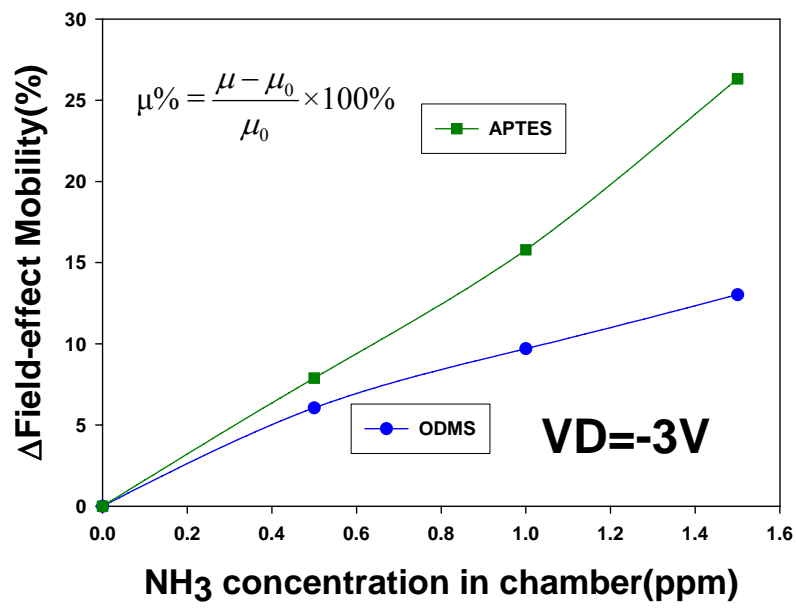
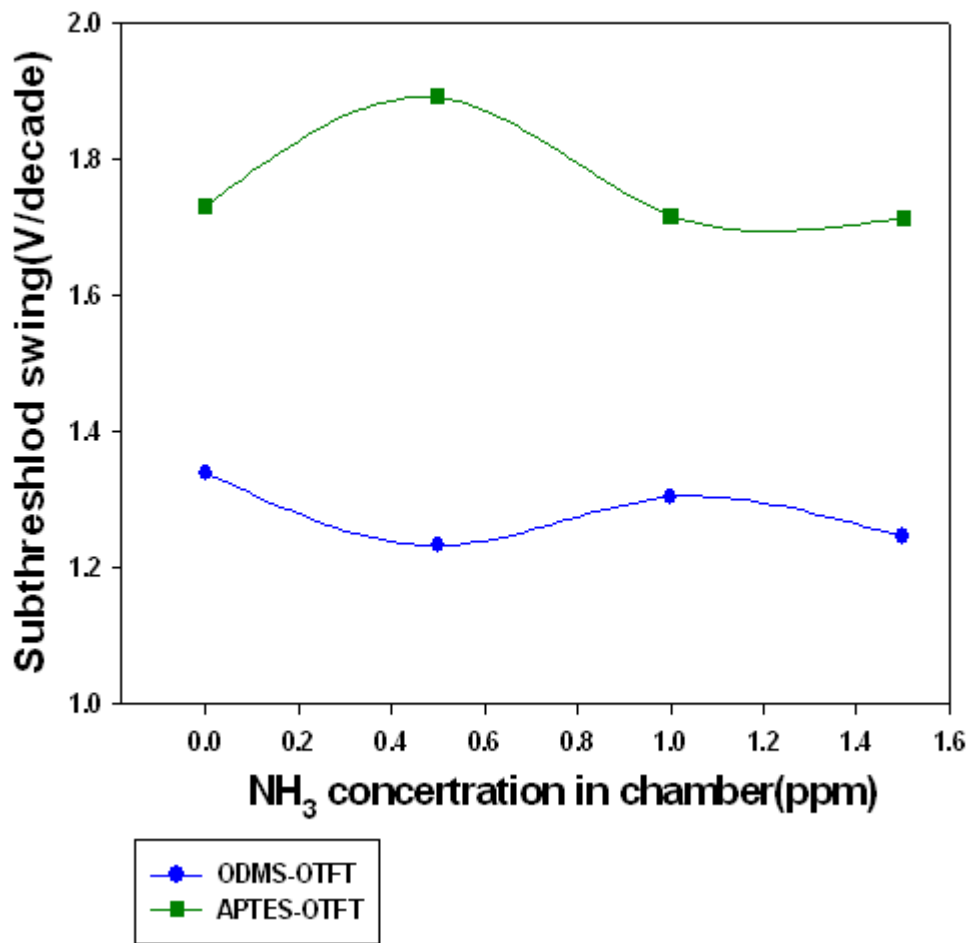


Fig. 4.9 The threshold voltage shift ( $\Delta V_{th}$ ) of ODMS and APTES-OTFTs is plotted as a function of NH<sub>3</sub> concentration.



**Fig. 4.10** The field-effect mobility of ODMS and APTES-OTFTs is plotted as a function of NH<sub>3</sub> concentration.





**Fig. 4.11** The subthreshold swing (*S.S.*) of ODMS and APTES-OTFTs is plotted as a function of NH<sub>3</sub> concentration.

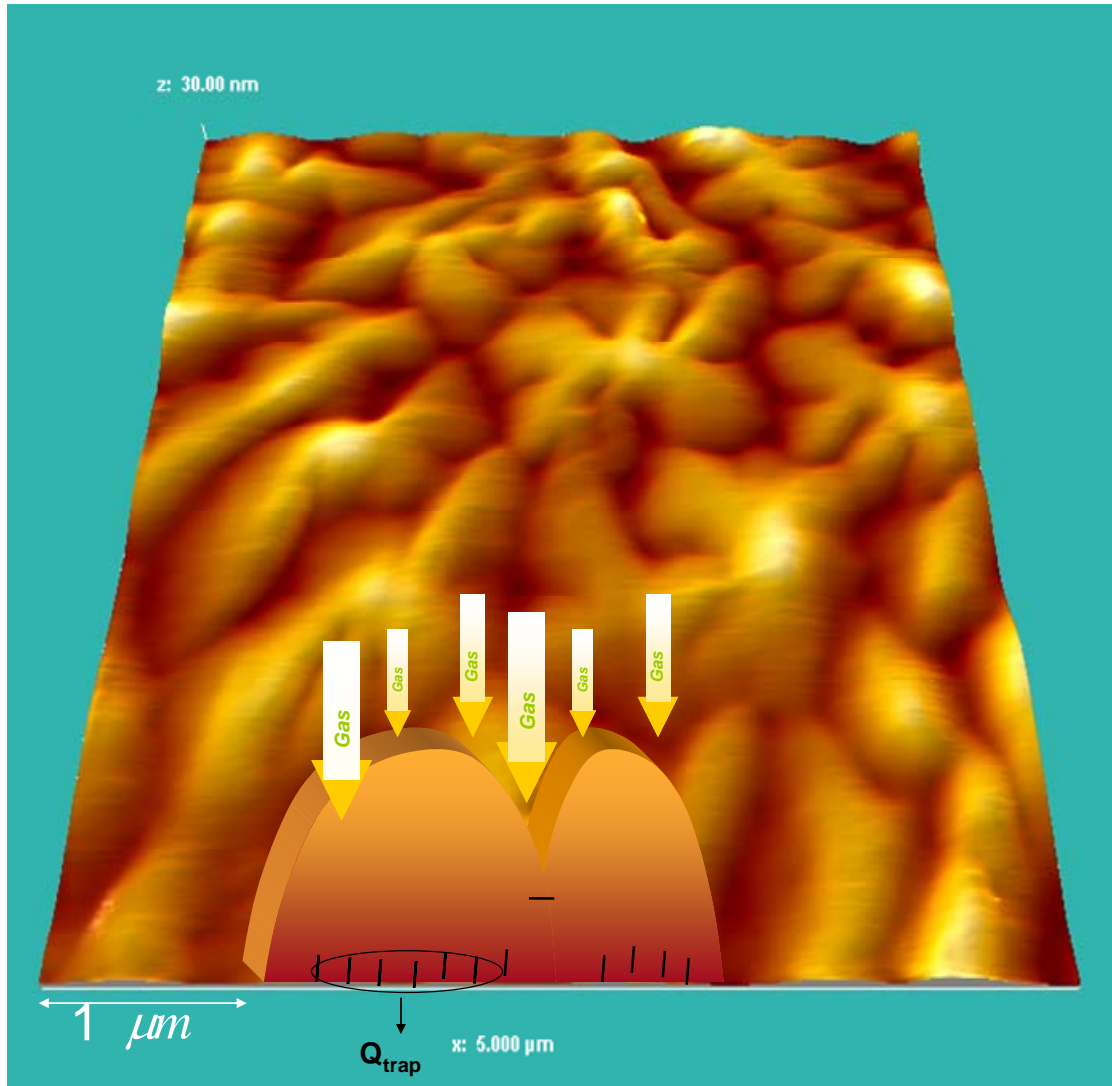


**Fig. 4.12** The sensing mechanism during  $\text{NH}_3$  in the chamber



# Chapter 5

## Conclusion and Future Work

### 5-1 Conclusion

In this thesis, we investigated that the influence of SAM on the surface energy. And propose the method to form the covalent bonding between APTES and BSA. Then, we discuss the comparison of electrical characteristics between ODMS and APTES-OTFTs. Finally, research the interaction of different SAM-treated OTFTs to  $\text{NH}_3$  gas via the gated-4-probes OTFTs in a gas-sensing system.

First of all, we study the surface characteristics of  $\text{SiO}_2$  which are modified by ODMS and APTES. The ODMS and APTES transformed the  $\text{SiO}_2$  surface from hydrophilic to hydrophobic, and ODMS and APTES do not affect the surface roughness significantly but the surface of ODMS mixed with APTES is rough obviously. Because of the above reasons, we choose ODMS and APTES as our main SAM in our experiments. We also propose the manner which can cause BSA and anti-body to form covalent bonding with APTES. According to AFM analysis of BSA and SEM analysis of anti-body with APTES or ODMS, we see the surface of BSA with APTES is uniform and the Au atoms on anti-body can be seen, but BSA with ODMS is not easy to be detected by AFM. Therefore, we deduce that  $-\text{NH}_2$  on APTES will bond to BSA, but there are no functional groups on ODMS which can

bond to BSA.

Further, we compare ODMS with APTES-OTFTs electrical characteristics. The threshold voltage of APTES-OTFTs with functional group (-NH<sub>2</sub>) is obviously higher than ODMS-OTFTs and the field-effect mobility of APTES-OTFTs is smaller than ODMS-OTFTs because of -NH<sub>2</sub> on APTES which can trap hole carriers to induce the low current and low mobility during on state.

Besides, in our observation, when ammonia (NH<sub>3</sub>) gas interacted with the OTFT, the threshold voltage is also shifted negatively to a larger value for both ODMS and APTES-OTFTs, and the field-effect mobility get lower with more NH<sub>3</sub>. However, the subthreshold swing was almost unchanged. We also propose that the percentage (%) of  $R_{cont}$  and  $R_{film}$  versus injected NH<sub>3</sub> and the percentage (%) of  $R_{film}$  is as high as about 90% during the NH<sub>3</sub> gaseous experiment for ODMS and APTES-OTFTs. Thus, we deduce the OTFT characteristics should be mainly dominated by the pentacene film properties rather than the contact properties.

We have proved that the functional groups, -NH<sub>2</sub>, on APTES affect electrical characteristics of OTFTs and electrical characteristics of OTFTs in ammonia. Through this thesis, we compare the sensitivity of ODMS and APTES-OTFTs in gas sensor. Finally, we hope to research more functional groups like -COOH, -SH to enhance the diversity of OTFTs sensing gas in the future.

## References

- [1] Frank-J. Meyer zu Heringdorf, M. C. Reuter and R. M. Tromp, "Growth dynamics of pentacene thin films," *Nature* 412, pp.517 (2001).
- [2] Y. Y. Lin, D. J. Gundlach, S. F. Nelson, and T. N. Jackson, "Pentacene organic thin-film transistors-molecular ordering and mobility", *IEEE Electron Device Lett.* vol. 18, pp. 87, (1997).
- [3] C. D. Dimitrakopoulos, and Patrick R. L. Malenfant, "Organic thin film transistors for large area electronics," *Adv. Mater.* 14(2), pp.109 (2002).
- [4] D. Knipp, R. A. Street, A. Völkel, and J. Ho, "Pentacene thin film transistors on inorganic dielectrics: Morphology, structural properties, and electronic transport," *J. Appl. Phys.* 93(1), pp.347 (2003).
- [5]. L. Torsi, A. Dodabalapur, L. J. Rothberg, A. W. P. Fung, H.E. Katz, "Performance Limits of Organic Transistors", *Science*, 1996, P 1462.
- [6]. H. E. Katz, C. Kloc, V. Sundar, J. Zaumseil, A. L. Briseno, Z. Bao, "Field-Effect Transistors made from Macroscopic Single Crystals of Teracene and Related Semiconductors on Polymer Dielectrics", *Journal of Material Research*, Vol. 19, No. 7, Jul 2004, P 1995 - 1998.
- [7]. C. D. Dimitrakopoulos, D. J. Mascaro, "Organic Thin-Film Transistors: A Review of Recent Advances", *IBM Journal of Research and Development*, Vol. 45, No. 1,

Jan 2001, P 11 - 27.

- [8] Z. Bao, A. Dodabalapur, A. J. Lovinger, "Soluble and processable regioregular poly(3-hexylthiophene) for thin film field-effect transistor applications with high mobility" Appl. Phys. Lett. Vol. 69, pp.4108, (1996)
- [9] Y.Y. Lin, D. J. Gundlach, S. Nelson, T. N. Jackson, "Stacked pentacene layer organic thin-film transistors with improved characteristics", IEEE Electron Device Lett, Vol. 18, pp.606, (1997).
- [10] Yanming Sun, Yunqi Liu, and Daoben Zhu, "Advances in organic field-effect transistors", J. Mater. Chem., vol. 15, pp. 53, (2005).
- [11] G. M. Wang, J. Swensen, D. Moses, and A. J. Heeger, "Increased mobility from regioregular poly (3-hexylthiophene) field-effect transistors", J. Appl. Phys, Vol 93, pp 6137, (2003)
- [12] L. Sebastian, G. Weiser, and H. Bassler, "Charge transfer transitions in solid tetracene and pentacene studied by electroabsorption", Chemical Physics, Vol 61, pp 125-135, (1981)
- [13] C.W. Chu, S.H. Li, C.W. Chen, V. Shrotriya, Y. Yang, "High-performance organic thin-film transistors with metal oxide/metal bilayer electrode" , Applied Physics Letters, Vol. 87, pp.193508, (2005)
- [14] E. A. Silinsh, and V.Capek, "Organic Molecular Crystals: Their Electronic States

“, New York, (1980)

[15] Y. S. Yang, S. H. Kim, J. Lee, H.Y. Chu, L. Do, “Deep-level defect characteristics in pentacene organic thin films”, Applied Physics Letters, Vol. 80, pp. 1595-1597, (2002)

[16] H. Yanagisawa, T. Tamaki, M. Nakamura, K. Kudo, “Structural and electrical characterization of pentacene films on SiO<sub>2</sub> grown by molecular beam” Thin Solid Films, Vol. 464-465, pp.398, (2004)

[17] D. Knipp, R. A. Street, A. Vo<sup>o</sup> lkel, J. Ho. “Pentacene thin film transistors on inorganic dielectrics: Morphology, structural properties, and electronic transport” Journal of Applied Physics, Vol. 93, pp.247, (2003)

[18] R. A. Street, D. Knipp, and A. R. Vo<sup>o</sup> lkel, “Hole transport in polycrystalline pentacene transistors”, Appl. Phys. Lett., vol. 80, pp. 1658, (2002).

[19] G. Horowitz, “Organic field-effect transistors”, Adv. Mater., vol. 10, pp. 365, (1998).

[20] Y.-Y. Lin, D. J. Gundlach, S. F. Nelson, and T. N. Jackson, “Stacked pentacene layer organic thin-film transistors with improved characteristics”, IEEE Electron Device Lett, vol. 18, pp 606, (2000).

[21] S. F. Nelson, Y.-Y. Lin, D. J. Gundlach, and T. N. Jackson, “Temperature-independent transport in high-mobility pentacene transistors”,

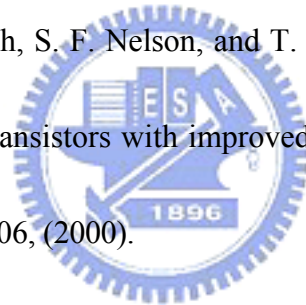
Appl. Phys. Lett., vol. 72, pp. 1854, (1998).

[22] O. Ostroverkhova, D. G. Cooke, S. Shcherbyna, R. F. Egerton, F. A. Hegmann, R. R. Tykwinski, and J. E. Anthony, “Bandlike transport in pentacene and functionalized pentacene thin films revealed by subpicosecond transient

[23] R. A. Street, D. Knipp, and A. R. Völkel, “Hole transport in polycrystalline pentacene transistors”, Appl. Phys. Lett., vol. 80, pp. 1658, (2002).

[24] G. Horowitz, “Organic field-effect transistors”, Adv. Mater., vol. 10, pp. 365, (1998).

[25] Y.-Y. Lin, D. J. Gundlach, S. F. Nelson, and T. N. Jackson, “Stacked pentacene layer organic thin-film transistors with improved characteristics”, IEEE Electron Device Lett, vol. 18, pp 606, (2000).



[26] Y.-Y. Lin, D. J. Gundlach, S. F. Nelson, and T. N. Jackson, “Stacked pentacene layer organic thin-film transistors with improved characteristics”, IEEE Electron Device Lett, vol. 18, pp 606, (2000).

[27] S. F. Nelson, Y.-Y. Lin, D. J. Gundlach, and T. N. Jackson, “Temperature-independent transport in high-mobility pentacene transistors”, Appl. Phys. Lett., vol. 72, pp. 1854, (1998).

[28] G. Nunes Jr., S. G. Zane, and J. S. Meth, “Styrenic polymers as gate dielectrics for pentacene field-effect transistors”, J. Appl. Phys., vol. 98, pp. 104503,

(2005).

[29] M. McDowell, I. G. Hill, J. E. McDermott, S. L. Bernasek, and J. Schwartz,

“Improved organic thin-film transistor performance using novel self-assembled monolayers”, *Appl. Phys. Lett.*, vol. 88, pp. 073505, (2006).

[30]. R.H. Tredgold, *Order in Thin Organic Films*, Cambridge University Press, 1994.

[31] A. Ulman, *An Introduction to Ultrathin Organic Films: From Langmuir-Blodgett to Self-Assembly*, Academic press, New York, 1991.

[32]. R.F. Gould (Ed.), *Contact Angle, Wettability and Adhesion*, Proceeding of the 144th Meeting of the American Chemical Society, Vol. 43, Washington, DC, 1964.



[33]. R.J. Good, Contact angle wetting and adhesion: a critical review, in: K.L. Mimal (Ed.), *Contact angle, Wettability and Adhesion*, USP, The Netherlands, 1993, pp. 3–36.

[34] Jeffrey T. Mabeck A George G. Malliaras, “**Chemical and biological sensors based on organic thin-film transistors**”, *Anal Bioanal Chem* (2006) 384: 343 – 353

[35] Qintao Zhang \*, Vivek Subramanian, “DNA hybridization detection with organic thin film transistors: Toward fast and disposable DNA microarray chips”  
, *Biosensors and Bioelectronics* 22 (2007) 3182–3187

- [36] Torsi et al., J. Phys. Chem. B (2002) Correlation between Oligothiophene Thin Film Transistor Morphology and Vapor Responses
- [37] Liang Wang, Daniel Fine, and Ananth Dodabalapur, Nanoscale chemical sensor based on organic thin-film transistors, APPLIED PHYSICS LETTERS VOLUME 85, NUMBER 26 27 DECEMBER 2004
- [38] B. Crone, A. Dodabalapur, A. Gelperin, L. Torsi, H. E. Katz, A. J. Lovinger, and Z. Bao, Electronic sensing of vapors with organic transistors, APPLIED PHYSICS LETTERS VOLUME 78, NUMBER 15 9 APRIL 2001
- [39] F. Liao, et al. "Organic TFTs as gas sensors for electronic nose applications", Sensors and Actuators B, Vol. 107, pp849-855, (2005)
- [40] B. Crone, A. Dodabalapur, A. Gelperin, L. Torsi, H. E. Katz, A. J. Lovinger, and Z. Bao, Electronic sensing of vapors with organic transistors, APPLIED PHYSICS LETTERS VOLUME 78, NUMBER 15 9 APRIL 2001
- [41] F. Liao, et al. "Organic TFTs as gas sensors for electronic nose applications", Sensors and Actuators B, Vol. 107, pp849-855, (2005)
- [42] Ferretti, S., Paynter, S., Russel, D.A., Sapsford, K.E., Richardson, D.J., 2000. Self-assembled monolayers; a versatile tool for the formulation of bio-surfaces. Trends Anal. Chem. 19, 530\_ 540.
- [43] Horng-Long Cheng, Yu-Shen Mai, Wei-Yang Chou, and Li-Ren Chang,



“Influence of molecular structure and microstructure on device performance of polycrystalline pentacene thin-film transistors”, Appl. Phys. Lett., vol. 90, pp. 171926, (2007).

[44] Qintao Zhang \*, Vivek Subramanian, DNA hybridization detection with organic thin film transistors: Toward fast and disposable DNA microarray chips, Biosensors and Bioelectronics 22 (2007) 3182–3187



# 簡歷

姓名：吳權陵

出生年月日：中華民國七十三年八月十一日

住址：彰化縣員林鎮大智街二十五巷六號

學歷：

國立中正大學物理系 (2002.09~2006.06)

國立交通大學光電工程研究所碩士 (2006.09~2008.06)



論文題目：

官能基修飾有機薄膜電晶體氣體感測之研究

**Functional Group Modification on Dielectric Interface of  
Pentacene-Based OTFTs for Ammonia Sensing Application**